

Causal hydrodynamic fluctuations in a one-dimensional expanding system

Shin-ei Fujii * and Tetsufumi Hirano †

Department of Physics, Sophia University, Tokyo 102-8554, Japan



(Received 27 October 2023; accepted 2 February 2024; published 27 February 2024)

We derive stochastic equations of motion of hydrodynamic fluctuations, performing perturbative expansion of the energy-momentum conservation equations around the boost invariant solution in a one-dimensional expanding system. In the course of derivation, we do not assume any specific forms of constitutive equations for shear stress tensor $\pi^{\mu\nu}$ and bulk pressure Π . Therefore, the framework enables us to employ any constitutive equations beyond the Navier-Stokes theory which satisfy the causality. Employing Israel-Stewart equations as examples of the constitutive equations, we demonstrate the dynamics of causal hydrodynamic fluctuations in (1+1)-dimensional Milne coordinates on an event-by-event basis. We observe that the structure of energy density and flow rapidity fluctuations is almost frozen in the early stage of the expansion. Two-point correlations of energy density fluctuations turn out to be closely related to the properties of the medium, such as sound velocity, viscosity, and relaxation time. Furthermore, we show that two-particle correlation functions of final hadrons after freeze-out inherit correlations of thermodynamic variables and flow rapidity. This opens a new door for an analysis of transport properties of the medium produced in relativistic heavy ion collisions.

DOI: [10.1103/PhysRevC.109.024916](https://doi.org/10.1103/PhysRevC.109.024916)

I. INTRODUCTION

One of the main goals of physics of relativistic heavy ion collisions is to reveal the bulk and the transport properties of the quark gluon plasma (QGP), namely, matter composed of quarks and gluons as elementary degrees of freedom under extremely high temperature and/or density. So far, a huge amount of experimental data on relativistic heavy ion collisions at the Relativistic Heavy Ion Collider (RHIC) and the Large Hadron Collider (LHC) has been reported. Relativistic ideal hydrodynamic models [1–7] greatly succeeded in describing the elliptic flow data at RHIC energies. Since then, relativistic hydrodynamics became a major framework to describe the space-time evolution of the QGP. We are now in the stage to sophisticate the dynamical model and to use it to extract the properties of the QGP more precisely.

Nowadays, relativistic dissipative hydrodynamics including shear and/or bulk viscosities has been used to extract transport properties of the QGP from experimental data through Bayesian parameter estimation [8–16]. Fluctuations and dissipations, however, always accompany each other according to the fluctuation-dissipation relations (FDR) in nonequilibrium statistical physics [17]. Since phenomena induced by the hydrodynamic fluctuations, namely, thermal fluctuations associated with the viscosities during hydrodynamic evolution, include the information of transport coefficients through FDRs, these provide a multidimensional analysis of transport properties of the QGP. Therefore, it is indispensable to incorporate hydrodynamic fluctuations in the dynamical framework of relativistic heavy ion collisions. This could open up a new way of diagnosing the QGP properties precisely.

In this paper, we formulate dynamics of causal hydrodynamic fluctuations in a one-dimensional expanding system [18], linearizing equations of energy-momentum conservation around the boost invariant solutions up to the first order without any assumption of specific constitutive equations. We also linearize causal constitutive equations including noise terms around the boost invariant solutions. We regard them as stochastic differential equations for hydrodynamic fluctuations. We demonstrate the event-by-event space-time evolution of fluctuations of thermodynamic variables and analyze the two-point correlation functions for them. To see the effects of hydrodynamic fluctuations in observables, we also analyze two-particle correlation functions of final hadrons.

Linearization of hydrodynamic equations under a boost invariant solution [18] has been performed in, e.g., Refs. [19,20] for analysis of stability and causality against perturbation. The first application of hydrodynamic fluctuations to the phenomenological model of relativistic heavy ion collisions was made in Ref. [21]. They linearized the relativistic hydrodynamic equations under boost invariant solutions [18] as backgrounds and regarded the first-order perturbative equations as equations of motion for hydrodynamic fluctuations. With these solutions, they obtained correlations of pion yield fluctuations in the rapidity direction. This study was further extended to (3+1)-dimensional expansion [22] by employing Gubser flow [23] as a background. However, both of them employed the first-order constitutive equations in which the gradient of flow velocity is included up to the first order for shear stress tensor $\pi^{\mu\nu}$ and bulk pressure Π . It is well known that relativistic hydrodynamic equations with first-order theory are classified as parabolic equations: The time derivative is of the first order while the space derivative is of the second order. Since the Green's function of parabolic equations is Gaussian and the long tail of it has a small but

*s-fujii-8c2@eagle.sophia.ac.jp

†hirano@sophia.ac.jp

finite value, the propagation speed of sound exceeds the speed of light (acausal). The first-order theory exhibits pathological behaviors and has not only an acausal problem but also instability [19,20,24–26]. Therefore, one has to extend its framework to the causal one [24,27–37] in the stage of sophistication to study the properties of the QGP more precisely.

The first attempt to develop a framework of causal hydrodynamic fluctuations in a (1+1)-dimensional expanding system was done in Ref. [38], in which constitutive equations at the Navier-Stokes limit in Ref. [21] were replaced with the second-order ones so that the system could obey the causality. Notice that ensemble averaged quantities were directly analyzed in Refs. [21,38]. Here we concentrate more on the analysis of event-by-event phenomena induced by hydrodynamic fluctuations and of transport properties of the QGP from spectra of particle identified hadrons as an event average. Instead of using the Green's function for the ensemble averaged quantities, we solve system of stochastic partial differential equations for each event. Furthermore, since hydrodynamics is an effective theory of the long wavelength limit, noise terms should be treated carefully to avoid singularities originated from short wavelengths. We tame such a nonphysical singularity, seen in Refs. [21,38], introducing a momentum cutoff for fluctuations in each event [39].

There have already been also several studies based on (3+1)-dimensional hydrodynamic models which include causal hydrodynamic fluctuations [39–46]. It is, however, quite difficult to intuitively understand what results from hydrodynamic fluctuations in heavy-ion collisions due to their complicated dynamics. Hence a relatively simpler geometry like (1+1)-dimensional boost invariance is particularly useful to understand the consequences of hydrodynamic fluctuations even if both viscosity and fluctuations are incorporated perturbatively [21,38]. Thus, a study of causal hydrodynamic fluctuations in a one-dimensional expanding system has a practical advantage over the full (3+1)-dimensional hydrodynamic simulations thanks to a much simpler framework. Since the hydrodynamic fluctuations originate from (local) thermal equilibrium, novel phenomena associated with hydrodynamic fluctuations would be clear and direct evidence of thermalization in relativistic heavy ion collisions.

The present paper is organized as follows: We derive a system of partial differential equations to describe the dynamics of causal hydrodynamic fluctuations in Sec. II. In Sec. III, we first discuss the validity of perturbation and then analyze the space-time evolution of thermodynamic variables and their correlations. We also calculate the two-particle correlation function of hadrons after freeze-out to see how the properties of the QGP affect observables. Section IV is devoted to a summary of the present study.

Throughout this paper, we use natural units, $\hbar = c = k_B = 1$, and the Minkowski metric, $g_{\mu\nu} = \text{diag}(1, -1, -1, -1)$.

II. MODEL

In this section, we derive equations of motion (EoMs) of causal hydrodynamic fluctuations in a (1+1)-dimensional expanding system. In Sec. II A, we first derive the equations of background and of perturbation in a one-dimensional

expanding system from the balance equations in relativistic hydrodynamics. We also perform perturbative expansion for constitutive equations with hydrodynamic fluctuations employing Israel-Stewart equations [27,28] in Sec. II B. We introduce fluctuation-dissipation relations (FDRs) in the Milne coordinate in Sec. II C. We discuss some other variables in the perturbative expansion in Sec. II D. We finally introduce models of the equation of state (EoS) and transport coefficients in Sec. II E. The formalism developed in this section is basically equivalent to the one in Ref. [38] besides event-by-event treatment of dynamics including momentum cutoff in the noises in our study.

A. Balance equations

Hydrodynamic balance equations are composed of conservation laws of energy, momentum, and charges. Throughout this paper, we neglect the conserved charges for simplicity. By means of tensor decomposition, the energy-momentum tensor, $T^{\mu\nu}$, can be expressed as

$$T^{\mu\nu} = eu^\mu u^\nu - (p + \Pi)\Delta^{\mu\nu} + \pi^{\mu\nu}, \quad (1)$$

where e , p , Π , and $\pi^{\mu\nu}$ are energy density, hydrostatic pressure, bulk pressure, and shear stress tensor, respectively. As a definition of flow velocity u^μ , we employ the Landau frame which satisfies an eigenvalue equation, $T^{\mu\nu}u^\nu = eu^\mu$. A projection tensor, $\Delta^{\mu\nu} \equiv g^{\mu\nu} - u^\mu u^\nu$, maps a four-vector to a space perpendicular to u^μ .

A boost invariant solution in (1+1)-dimensional space for relativistic hydrodynamic equations is written as [18]

$$u_{\text{Bj}}^\mu = \frac{t}{\tau} \left(1, 0, 0, \frac{z}{t} \right) = (\cosh \eta_s, 0, 0, \sinh \eta_s), \quad (2)$$

where $\tau \equiv \sqrt{t^2 - z^2}$ and $\eta_s \equiv \tanh^{-1}(z/t)$ are proper time and space-time rapidity, respectively. This solution exhibits the one-dimensional Hubble-like expansion along the collision axis (z axis), intrinsically holds boost invariant property, and, as a result, thermodynamic variables do not depend on η_s .

In order to perform perturbative expansion around boost invariant solutions, we first assume small deviations of flow velocity. Flow velocity with small flow rapidity, $\delta y(\tau, \eta_s)$, is

$$\begin{aligned} u^\mu &= (\cosh[\eta_s + \delta y(\tau, \eta_s)], 0, 0, \sinh[\eta_s + \delta y(\tau, \eta_s)]) \\ &\approx (\cosh \eta_s, 0, 0, \sinh \eta_s) + (\sinh \eta_s, 0, 0, \cosh \eta_s)\delta y \\ &\equiv u_{(0)}^\mu(\eta_s) + u_{(1)}^\mu(\tau, \eta_s), \end{aligned} \quad (3)$$

where subscripts (0) and (1) denote the zeroth and the first order in perturbation, respectively. Correspondingly, thermodynamic variables and dissipative currents in the energy-momentum tensor (1) can be expanded as

$$e \approx e_{(0)}(\tau) + e_{(1)}(\tau, \eta_s), \quad (4)$$

$$p \approx p_{(0)}(\tau) + p_{(1)}(\tau, \eta_s), \quad (5)$$

$$\Pi \approx \Pi_{(0)}(\tau) + \Pi_{(1)}(\tau, \eta_s), \quad (6)$$

$$\pi^{\mu\nu} \approx \pi_{(0)}^{\mu\nu}(\tau) + \pi_{(1)}^{\mu\nu}(\tau, \eta_s). \quad (7)$$

Here the variables with subscript (0) are independent of η_s because of the boost invariant property of backgrounds.

Consequently, some other quantities become

$$\begin{aligned}\Delta^{\mu\nu} &= g^{\mu\nu} - u^\mu u^\nu \approx g^{\mu\nu} - u_{(0)}^\mu u_{(0)}^\nu - u_{(0)}^\mu u_{(1)}^\nu - u_{(1)}^\mu u_{(0)}^\nu \\ &\equiv \Delta_{(0)}^{\mu\nu} + \Delta_{(1)}^{\mu\nu},\end{aligned}\quad (8)$$

$$\mathcal{D} = u^\mu \partial_\mu \approx \frac{\partial}{\partial \tau} + \frac{\delta y}{\tau} \frac{\partial}{\partial \eta_s} \equiv \mathcal{D}_{(0)} + \mathcal{D}_{(1)},\quad (9)$$

$$\begin{aligned}\nabla^\alpha &= \Delta^{\alpha\mu} \partial_\mu \approx \partial^\alpha - u_{(0)}^\alpha \mathcal{D}_{(0)} - u_{(1)}^\alpha \mathcal{D}_{(0)} - u_{(0)}^\alpha \mathcal{D}_{(1)} \\ &\equiv \nabla_{(0)}^\alpha + \nabla_{(1)}^\alpha,\end{aligned}\quad (10)$$

$$\theta = \partial_\mu u^\mu \approx \frac{1}{\tau} + \frac{1}{\tau} \frac{\partial}{\partial \eta_s} \delta y \equiv \theta_{(0)} + \theta_{(1)}.\quad (11)$$

Here a partial derivative is decomposed as $\partial^\mu = u^\mu \mathcal{D} + \nabla^\mu$ and θ is an expansion scalar. Substituting these variables and differential operators into balance equations of the energy and momentum, $\partial_\mu T^{\mu\nu} = 0$, we derive the EoMs of backgrounds and of fluctuations in a one-dimensional expanding system. Timelike and spacelike parts of the energy-momentum conservation are, respectively,

$$u_\nu \partial_\mu T^{\mu\nu} = 0,\quad (12)$$

$$\Delta_{\alpha\nu} \partial_\mu T^{\mu\nu} = 0.\quad (13)$$

From Eq. (12), we obtain

$$De + (e + p + \Pi)\theta - \pi_{\mu\nu} \partial^{(\mu} u^{\nu)} = 0,\quad (14)$$

where angle brackets in the third term stand for the following operation for any second-rank tensor $A^{\mu\nu}$:

$$\begin{aligned}A^{(\mu\nu)} &\equiv \Delta^{\mu\nu}{}_{\alpha\beta} A^{\alpha\beta}, \\ &= \left[\frac{1}{2} (\Delta^\mu{}_\alpha \Delta^\nu{}_\beta + \Delta^\nu{}_\alpha \Delta^\mu{}_\beta) - \frac{1}{3} \Delta^{\mu\nu} \Delta_{\alpha\beta} \right] A^{\alpha\beta}.\end{aligned}\quad (15)$$

The resultant tensor becomes symmetric, traceless, and transverse to flow velocity. Inserting thermodynamic variables and differential operators up to the first order in perturbation into Eq. (14), we obtain

$$\text{0th: } \frac{d}{d\tau} e_{(0)} + \frac{1}{\tau} (e_{(0)} + p_{(0)} + \Pi_{(0)} - \pi_{(0)}) = 0,\quad (16)$$

$$\begin{aligned}\text{1st: } \frac{\partial}{\partial \tau} e_{(1)} + \frac{1}{\tau} (e_{(1)} + p_{(1)} + \Pi_{(1)} - \pi_{(1)}) \\ + \frac{1}{\tau} \frac{\partial}{\partial \eta_s} \delta y (e_{(0)} + p_{(0)} + \Pi_{(0)} - \pi_{(0)}) = 0,\end{aligned}\quad (17)$$

where we separate equations order by order and define shear pressure π as

$$\pi \equiv \pi^{00} - \pi^{33} \approx \pi_{(0)}(\tau) + \pi_{(1)}(\tau, \eta_s).\quad (18)$$

The zeroth-order equation (16) describes the time evolution of background energy density. This equation is nothing but the Bjorken equation with viscosity. The first and the second terms in the left-hand side of Eq. (17) share the same form as those in Eq. (16), while the third term appears as a consequence of linearization. The additional third term contains a gradient of fluctuations of flow rapidity with respect to η_s and describes longitudinal dynamics of fluctuations. Thus, the system is no longer boost invariant.

From Eq. (13), we derive EoMs of flow velocity:

$$(e + p + \Pi) \mathcal{D} u^\alpha - \nabla^\alpha (p + \Pi) + \Delta^\alpha{}_\nu \partial_\mu \pi^{\mu\nu} = 0.\quad (19)$$

Following the same prescription as above, we finally obtain,¹

$$\text{0th: } \frac{\partial}{\partial \eta_s} (p_{(0)} + \Pi_{(0)} - \pi_{(0)}) = 0,\quad (20)$$

$$\begin{aligned}\text{1st: } \frac{\partial}{\partial \tau} \delta y (e_{(0)} + p_{(0)} + \Pi_{(0)} - \pi_{(0)}) \\ + \frac{2\delta y}{\tau} (e_{(0)} + p_{(0)} + \Pi_{(0)} - \pi_{(0)}) \\ + \frac{1}{\tau} \frac{\partial}{\partial \eta_s} (p_{(1)} + \Pi_{(1)} - \pi_{(1)}) = 0.\end{aligned}\quad (21)$$

The zeroth-order equation (20) gives a condition for the background pressure and dissipative currents to be boost invariant. Therefore, this equation can be neglected as long as we implicitly assume a boost invariant property of backgrounds. As seen in Eq. (17), a gradient with respect to η_s appears in the third term of Eq. (21): The flow rapidity fluctuations are induced by the spatial gradient of fluctuations of total pressure, $p_{(1)} + \Pi_{(1)} - \pi_{(1)}$. Since we do not assume any specific forms of constitutive equations, these balance equations obtained above, Eqs. (16)–(21), are generic and are used for any models of phenomenological constitutive equations.

B. Constitutive equations with noises

In this paper, we employ the simplest causal constitutive equations derived by Israel and Stewart [27,28] for the purpose of demonstration of the current framework,²

$$\pi^{\mu\nu} + \Delta^{\mu\nu}{}_{\alpha\beta} \tau_\pi \mathcal{D} \pi^{\alpha\beta} = 2\eta \nabla^{(\mu} u^{\nu)} + \xi_\pi^{\mu\nu},\quad (22)$$

$$(1 + \tau_\Pi \mathcal{D}) \Pi = -\zeta \theta + \xi_\Pi,\quad (23)$$

where noise terms $\xi_\pi^{\mu\nu}(\tau, \eta_s)$ and $\xi_\Pi(\tau, \eta_s)$ for shear stress tensor and bulk pressure, respectively, are introduced as hydrodynamic fluctuations. Here transport coefficients η , ζ , τ_π , and τ_Π are shear viscosity, bulk viscosity, relaxation time for shear stress tensor, and relaxation time for bulk pressure, respectively. Since the transport coefficients are, in general, functions of temperature, which has boost invariant background and small fluctuations through the EoS, the transport coefficients can be also decomposed into the boost invariant zeroth-order terms and the space-time rapidity dependent first-order terms as fluctuations:

$$\eta \approx \eta_{(0)}(\tau) + \eta_{(1)}(\tau, \eta_s),\quad (24)$$

$$\zeta \approx \zeta_{(0)}(\tau) + \zeta_{(1)}(\tau, \eta_s),\quad (25)$$

$$\tau_\pi \approx \tau_{\pi(0)}(\tau) + \tau_{\pi(1)}(\tau, \eta_s),\quad (26)$$

$$\tau_\Pi \approx \tau_{\Pi(0)}(\tau) + \tau_{\Pi(1)}(\tau, \eta_s).\quad (27)$$

¹Actually, we obtain two equations which correspond to $\alpha = 0$ and 3 in Eq. (19). Linear combination of them results in this equation.

²These equations are often called ‘‘simplified Israel-Stewart equations.’’ It is, however, not a precise name to describe these equations since what they actually showed in their papers are indeed these equations. ‘‘Israel-Stewart equations’’ in the recent literature were obtained first by Hiscock and Lindbrom [24].

With these assumptions, we finally obtain the constitutive equations for shear pressure, π , as

$$\text{0th : } \pi_{(0)} + \tau_{\pi(0)} \frac{d}{d\tau} \pi_{(0)} = \frac{4\eta_{(0)}}{3\tau}, \quad (28)$$

$$\begin{aligned} \text{1st : } \pi_{(1)} + \tau_{\pi(0)} \frac{\partial}{\partial \tau} \pi_{(1)} + \tau_{\pi(1)} \frac{d}{d\tau} \pi_{(0)} \\ = \frac{4\eta_{(1)}}{3\tau} + \frac{4\eta_{(0)}}{3\tau} \frac{\partial}{\partial \eta_s} \delta y + \xi_\pi, \end{aligned} \quad (29)$$

where, for both the zeroth-order and the first-order perturbative equations, shear stress tensor $\pi^{\mu\nu}$ in Eq. (22) is simply reduced to $\pi_{(0)} = \pi_{(0)}^{00} - \pi_{(0)}^{33}$ and $\pi_{(1)} = \pi_{(1)}^{00} - \pi_{(1)}^{33}$ within the present assumptions. The noise term ξ_π is also defined as $\xi_\pi \equiv \xi_\pi^{00} - \xi_\pi^{33}$. Similarly, the constitutive equations for bulk pressure Π are obtained as

$$\text{0th : } \Pi_{(0)} + \tau_{\Pi(0)} \frac{d}{d\tau} \Pi_{(0)} = -\frac{\zeta_{(0)}}{\tau}, \quad (30)$$

$$\begin{aligned} \text{1st : } \Pi_{(1)} + \tau_{\Pi(0)} \frac{\partial}{\partial \tau} \Pi_{(1)} + \tau_{\Pi(1)} \frac{d}{d\tau} \Pi_{(0)} \\ = -\frac{\zeta_{(1)}}{\tau} - \frac{\zeta_{(0)}}{\tau} \frac{\partial}{\partial \eta_s} \delta y + \xi_\Pi. \end{aligned} \quad (31)$$

In the course of derivation, we regarded noise terms ξ_π and ξ_Π as variables at the first order [21,38]. In other words, fluctuations of thermodynamic variables on top of boost-invariant background are induced directly ($\pi_{(1)}$ and $\Pi_{(1)}$) or indirectly ($e_{(1)}$ and δy) by hydrodynamic fluctuations.

C. Fluctuation-dissipation relation

We next set the power of noises and their probability distributions. When the background medium keeps local equilibrium but dynamically evolves, as is often assumed in the space-time evolution in relativistic heavy ion collisions, it is not trivial whether the ordinary FDRs can be used. The FDR was generalized in such a case in Ref. [47]. Although we should have employed this generalized version of FDR in the current setting, we postpone analysis of the effect of generalization to future work and employ the ordinary FDR in this study.

From the consequences of nonequilibrium statistical physics, Gaussian white noises, ξ_π and ξ_Π , obey the following FDRs in the Milne coordinate [48]:

$$\langle \xi_\pi(x) \rangle = 0, \quad (32)$$

$$\begin{aligned} \langle \xi_\pi(x) \xi_\pi(x') \rangle &= \frac{8\eta_{(0)} T_{(0)}}{3} \delta^4(x - x') \\ &= \frac{8\eta_{(0)} T_{(0)}}{3\tau} \delta(\tau - \tau') \delta(\eta_s - \eta'_s) \delta^2(\mathbf{x}_\perp - \mathbf{x}'_\perp), \end{aligned} \quad (33)$$

$$\langle \xi_\Pi(x) \rangle = 0, \quad (34)$$

$$\begin{aligned} \langle \xi_\Pi(x) \xi_\Pi(x') \rangle &= 2\zeta_{(0)} T_{(0)} \delta^4(x - x') \\ &= \frac{2\zeta_{(0)} T_{(0)}}{\tau} \delta(\tau - \tau') \delta(\eta_s - \eta'_s) \delta^2(\mathbf{x}_\perp - \mathbf{x}'_\perp), \end{aligned} \quad (35)$$

where $T_{(0)}$ is the temperature of the background and $\mathbf{x}_\perp \equiv (x, y)$ are transverse coordinates. Regarding the FDR of shear pressure (33), the original form has four Lorentz indices,

$$\langle \xi_\pi^{\mu\nu}(x) \xi_\pi^{\alpha\beta}(x') \rangle = 4\eta_{(0)} T_{(0)} \delta^4(x - x') \Delta^{\mu\nu\alpha\beta}. \quad (36)$$

Under the present situations, the noise term is, however, no longer a tensor, and is reduced to $\xi_\pi(x) \equiv \xi_\pi^{00}(x) - \xi_\pi^{33}(x)$ due to the symmetry. Thus, Eq. (33) can be obtained from Eq. (36) through the following calculations:

$$\begin{aligned} \langle \xi_\pi(x) \xi_\pi(x') \rangle &= \langle (\xi_\pi^{00}(x) - \xi_\pi^{33}(x)) (\xi_\pi^{00}(x') - \xi_\pi^{33}(x')) \rangle \\ &= 4\eta_{(0)} T_{(0)} \delta^4(x - x') (\Delta^{0000} + \Delta^{3333} - \Delta^{0033} - \Delta^{3300}) \\ &= \frac{8\eta_{(0)} T_{(0)}}{3} \delta^4(x - x'). \end{aligned} \quad (37)$$

When it comes to solving the stochastic differential equations numerically, both space and time should be discretized by introducing finite time step $\Delta\tau$ and cell size $\Delta\eta_s$. Regarding FDRs (33) and (35), delta functions should be also discretized by the following replacement:

$$\delta(\tau - \tau') \rightarrow \frac{\delta_{\tau\tau'}}{\Delta\tau}, \quad (38)$$

$$\delta^2(\mathbf{x}_\perp - \mathbf{x}'_\perp) \rightarrow \frac{1}{\Delta x \Delta y}, \quad (39)$$

$$\delta(\eta_s - \eta'_s) \rightarrow G(\eta_s - \eta'_s) \equiv \frac{1}{\sqrt{2\pi\sigma_{\eta_s}^2}} \exp\left(-\frac{(\eta_s - \eta'_s)^2}{2\sigma_{\eta_s}^2}\right), \quad (40)$$

where the delta function of η_s is replaced with a Gaussian function with finite standard deviation σ_{η_s} so that spatially smeared noises are generated [39]. To avoid singularities originating from short wavelengths of hydrodynamic fluctuations, we introduce momentum the cutoff, $1/\sigma_{\eta_s}$. This essentially suppresses the higher wave numbers (momenta) of noises in the space-time rapidity direction. For the time integration of stochastic differential equations, the second-order stochastic Runge-Kutta method is employed [48,49].

Throughout this paper, we set $\Delta\tau = 0.01$ fm, $\Delta x = \Delta y = 2$ fm, $\Delta\eta_s = 0.1$, and $\sigma_{\eta_s} = 0.1$. We introduce the smearing of hydrodynamic noises with a cutoff parameter ($=5\sigma_{\eta_s}$) and the noises are no longer correlated beyond the cutoff parameter length in the space-time rapidity direction. The region of space-time rapidity is defined in $\eta_{s,\min} \leq \eta_s \leq \eta_{s,\max}$ with $\eta_{s,\min} = 0$ and $\eta_{s,\max} = 10$. We employ periodic boundary conditions of the first-order variables, $e_{(1)}(\eta_s = \eta_{s,\min}) = e_{(1)}(\eta_s = \eta_{s,\max})$, and so on in the numerical calculations.

D. Other variables

In order to deal with the first-order variables of transport coefficients, we assume they depend on temperature and convert variables into fluctuations of energy density $e_{(1)}$.

Then, the first-order variables of transport coefficients are written as

$$\tau_{\pi(1)}(T) = \frac{\partial \tau_{\pi(0)}(T)}{\partial T} \frac{\partial T}{\partial e_{(0)}} e_{(1)}, \quad (41)$$

$$\tau_{\Pi(1)}(T) = \frac{\partial \tau_{\Pi(0)}(T)}{\partial T} \frac{\partial T}{\partial e_{(0)}} e_{(1)}, \quad (42)$$

$$\eta_{(1)}(T) = \frac{\partial \eta_{(0)}(T)}{\partial T} \frac{\partial T}{\partial e_{(0)}} e_{(1)}, \quad (43)$$

$$\zeta_{(1)}(T) = \frac{\partial \zeta_{(0)}(T)}{\partial T} \frac{\partial T}{\partial e_{(0)}} e_{(1)}. \quad (44)$$

Here $\partial e_{(0)}/\partial T \equiv c_V(T)$ is heat capacity per unit volume. Once specific models of transport coefficients are given, the first-order variables can be treated in this way.

The first-order term of hydrostatic pressure is obtained after a specific model of the EoS, $p = p(e)$, is given as

$$p_{(1)} = \frac{\partial p_{(0)}}{\partial e_{(0)}} e_{(1)} = c_s^2 e_{(1)}, \quad (45)$$

where c_s^2 is the square of sound velocity.

E. Models of EoS and transport coefficients

In the following, we specify models of EoS and transport coefficients. We employ two models of the EoS: the conformal EoS, $p = \frac{1}{3}e$, with the degrees of freedom $d = 47.5$, for massless $N_f = 3$ QCD as one model, and a parametrization of lattice EoS results [50] as the other model. In the case of conformal EoS, bulk pressure Π vanishes because of conformal symmetry. Hence we also neglect the bulk pressure Π even in the case of lattice EoS for comparison and focus on the shear pressure π as a dissipative current. For the transport coefficients, we choose the specific shear viscosity $\eta/s = 1/4\pi$ [51] and relaxation time $\tau_\pi = (2 - \ln 2)/2\pi T$ [30] obtained from AdS/CFT correspondence. These parameters are used as a default setting. When we investigate parameter dependence on final results, we multiply these transport coefficients by a constant factor.

III. RESULTS

In what follows, we change the notation of background energy density as $e_{(0)} \rightarrow e_0$ and a fluctuation of energy density as $e_{(1)} \rightarrow \delta e$, for simplicity. Then, the total energy density of the system is written as $e(\tau, \eta_s) = e_0(\tau) + \delta e(\tau, \eta_s)$. The notation of the other variables is also changed accordingly. Since the equations to be solved are first-order differential equations in time, we need to assign initial conditions for each variable. We start the hydrodynamic evolution at initial time $\tau_{\text{ini}} = 1$ fm. Initial conditions are summarized in Table I. These initial conditions are commonly used throughout this paper.³ The smooth initial conditions with vanishing fluctuations are chosen in the longitudinal direction. We plan to

³When we study effects of transport coefficients on final results by multiplying a factor with the shear viscosity η_0 in Figs. 6 and 11, the initial conditions for π_0 are also changed accordingly.

TABLE I. Initial conditions.

Variables	Values
τ	1 fm
e_0	10 GeV/fm ³
π_0	$4\eta_0/3\tau_{\text{ini}}$ GeV/fm ³
δe	0 GeV/fm ³
$\delta\pi$	0 GeV/fm ³
δy	0

investigate the effects of initial longitudinal fluctuations on final observables in future publications.

Before going into details on the results, we discuss how the sound wave propagates in a one-dimensional expanding system in Appendix A. The property of sound propagation in a one-dimensional expanding system is totally different from that of a static medium. When the reference of the frame moves at some constant speed, one observes the sound horizon. On the other hand, when the background medium expands, one sees that the information of fluctuations reaches infinity in η_s space. These are helpful in understanding how the individual fluctuation induced by thermal noises propagates in the space-time rapidity direction.

A. Validity of perturbation

First, we discuss the validity of perturbation and clarify the applicability of our model. Since we linearized the EoMs under the assumption that fluctuations are sufficiently smaller than backgrounds, we need to care about the magnitude of fluctuations. Figure 1 shows the time evolution of the absolute values of the ratios (a) $|\delta e/e_0|$, (b) $|\delta y|$, and (c) $|\delta\pi/\pi_0|$. Here the magnitude of fluctuation of flow rapidity, δy , should be compared to just unity since flow velocity (3) in the comoving system ($y = \eta_s$) is

$$u_{\text{comoving}}^\mu = (1, 0, 0, \delta y). \quad (46)$$

It is clear that the ratios are always smaller than 0.1 for energy density and flow rapidity, while the ratio of shear pressure monotonically increases and exceeds unity at $\tau \approx 4$ fm in the case of conformal EoS and default transport coefficients. On the other hand, in the case of lattice EoS, it exceeds unity at $\tau \approx 2.5$ fm. To understand the EoS dependence of the behaviors of $|\delta\pi/\pi_0|$ in Fig. 1(c), let us analytically assess the time dependence of $|\xi_\pi|/\pi_0$ instead of $\delta\pi/\pi_0$ by assuming a model EoS, $p = c_s^2 e$, and shear viscosity, $\eta/s = 1/4\pi$, at the first order theory. First, time dependence of π_0 can be estimated as

$$\pi_0 = \frac{4\eta_0}{3\tau} \propto s_0 \times \tau^{-1} \propto \tau^{-2}, \quad (47)$$

where s_0 is the entropy density of the background and the effect of entropy production on time dependence can be neglected. On the other hand, time dependence of the standard deviation of noise ξ_π can be given by the FDR (33),

$$|\xi_\pi| \approx \langle \xi_\pi \xi_\pi \rangle^{\frac{1}{2}} \propto \left(\frac{\eta_0 T_0}{\tau} \right)^{\frac{1}{2}} \propto (s_0 T_0 \tau^{-1})^{\frac{1}{2}} \propto \tau^{-1-\frac{1}{2}c_s^2}. \quad (48)$$

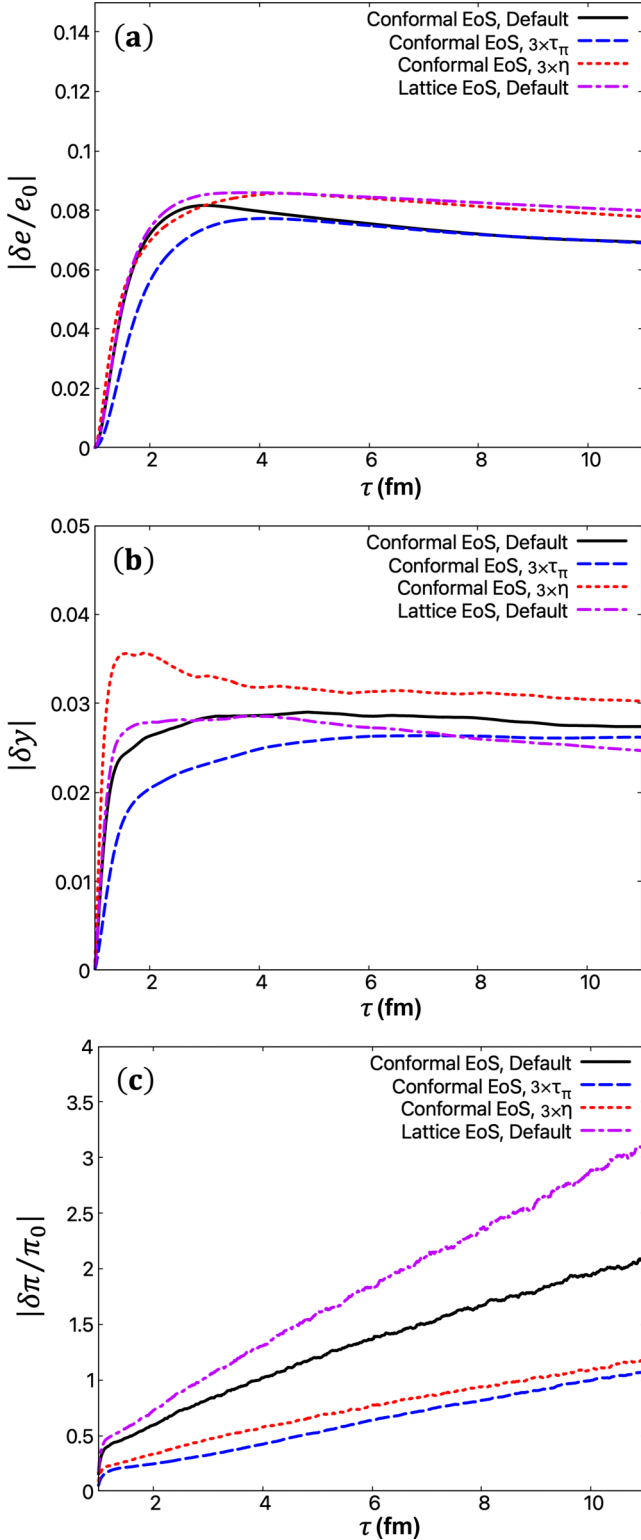


FIG. 1. Absolute values of the ratio of average fluctuations and background. Time evolution of (a) energy density, (b) flow rapidity, and (c) shear pressure are shown in comparison. The black solid line, blue dashed line, red dotted line, and magenta dash-dotted line are results from conformal EoS with default transport coefficients, conformal EoS with three times larger τ_π , conformal EoS with three times larger η , and lattice EoS with default transport coefficients, respectively. All results are averaged over 10 000 events at $\eta_s = 5.0$.

Therefore, time dependence of a typical value of the ratio $|\xi_\pi|/\pi_0$ leads to

$$\frac{|\xi_\pi|}{\pi_0} \propto \tau^{1-\frac{1}{2}c_s^2}. \quad (49)$$

Since the power of τ in Eq. (49) is always positive, $1 - \frac{1}{2}c_s^2 \geq 0$, the ratio monotonically increases with proper time, and fluctuations become dominant against the background shear pressure eventually.⁴ Moreover, the softer the EoS is, the more rapidly the ratio increases. This is the reason why the ratio with lattice EoS increases more rapidly than the one with conformal EoS. When it becomes larger than unity, this framework breaks down.

The stability condition of the thermal state is nothing but the FDR. Thus, in the thermal bath, the background shear stress tensor vanishes on average, while fluctuations of it always exist due to thermal fluctuations. Since the expansion rate of the volume decreases as $\theta \approx \tau^{-1}$ in a one-dimensional expanding system, it is inevitable that the fluctuations of shear pressure becomes larger than its background and that the current framework eventually breaks down.

As a possible makeshift prescription to this issue, we may use larger values of Δx and Δy in Eq. (39) to suppress the noise, or use larger initial conditions for background. As seen in Fig. 1, the larger the chosen transport coefficients are, the better the perturbative treatment is. This can be understood from Eqs. (47) and (48) since the ratio becomes

$$\frac{|\xi_\pi|}{\pi_0} \propto \frac{1}{\sqrt{\eta_0}} \quad (50)$$

at a fixed time.

Although we should have had to pay attention to the behavior of shear pressure in the present study, we postpone a detailed analysis of conditions for the validity of perturbation to a future publication, which includes reformulation of equation of motion for shear pressure. In Sec. III D, we will boldly use the information in the later stage under hydrodynamic evolution with lattice EoS when we calculate two-particle correlation functions, which might not have been justified from a viewpoint of validity conditions discussed in this section.

B. Space-time evolution

Next, let us exhibit numerical solutions of a system of stochastic partial differential equations obtained in the previous section. First, we describe the space-time evolution of thermodynamic variables, which is a sum of the background and fluctuations. Figure 2 shows the time evolution of energy density distribution from one sampled event.⁵ It is evident that the background energy density decreases immediately from the initial value, $e_0(\tau = 1 \text{ fm}) = 10 \text{ GeV}/\text{fm}^3$, due to the rapid expansion of the system. Through a system of partial differential equations, the fluctuations of energy density

⁴The actual power would be corrected due to the production of entropy. Nevertheless, the conclusion does not change here.

⁵The tendencies of time evolution exhibited in this subsection are quite common in other sampled events.

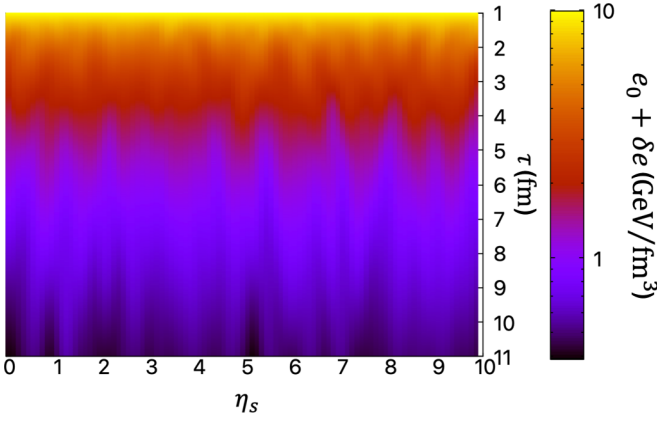


FIG. 2. Space-time evolution of total energy density in an event as an example. Time passes from top to bottom and the color bar indicates the magnitude of energy density.

are induced by hydrodynamic fluctuations: Hydrodynamic fluctuations induce the fluctuations of shear pressure, $\delta\pi$, which gives a space-time rapidity dependent $p dV$ work; on the other hand, fluctuations of flow rapidity, δy , also give a space-time dependent expansion rate of local volume, $\delta\theta$. A crucial thing is that a streak-like structure appears through the time evolution and is kept until the final time $\tau = 11$ fm. It means that the pattern of energy density distribution is almost frozen during the evolution and could carry the information of the early stage. One of the possible reasons for such a phenomenon is the interplay between the diffusion of fluctuations due to the finite shear viscosity and the effect of stretching the fluctuations due to the rapid expansion of the system. That is to say, the phenomenon “freeze of distribution” is an intrinsic property of an expanding system. To our best knowledge, it is shown for the first time that hydrodynamic fluctuations lead to structure formation of matter created in relativistic heavy ion collisions.

In Fig. 3, a similar structure appears in the case of flow rapidity fluctuations. From Eq. (21), it is induced by the spatial gradient of fluctuations of energy density, δe , and those of

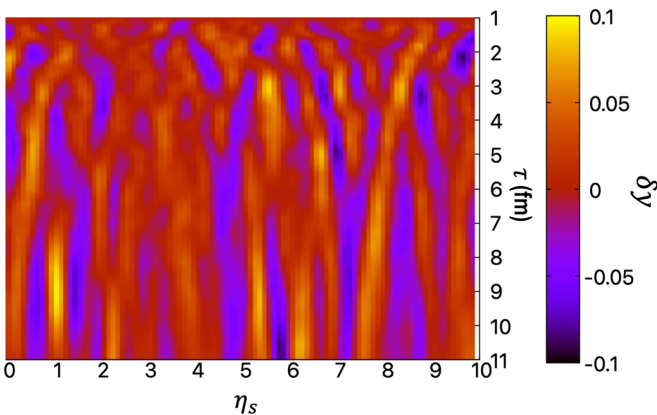


FIG. 3. Space-time evolution of flow rapidity fluctuations in the same event as in Fig. 2. Time passes from top to bottom and the color bar indicates the magnitude of flow rapidity fluctuations.

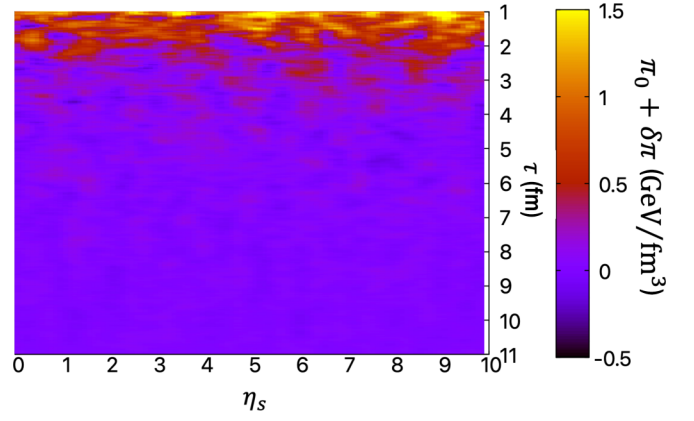


FIG. 4. Space-time evolution of total shear pressure in the same event as in Fig. 2. Time passes from top to bottom and the color bar indicates the magnitude of shear pressure.

shear pressure $\delta\pi$. The gradient of energy density fluctuations persists throughout the time evolution. Note that we plotted only flow rapidity fluctuations, δy , rather than the total flow rapidity in Fig. 3 since we are interested in deviation from Bjorken’s solution (2).

Figure 4 shows the space-time evolution of shear pressure. In contrast to the case of energy density or flow rapidity, there is no such a streak-like structure in the shear pressure. Shear pressure is known as a “fast variable,” namely, fluctuations of shear pressure are damped very quickly since it is not a conserved variable. This is one of the main reasons why the streak-like structure cannot be observed in the space-time evolution of shear pressure.

C. Correlations of fluctuations

Next, we investigate correlations of fluctuations and their dependence on various settings. Figure 5 shows the relaxation time dependence of two-point correlation functions of normalized energy density at (a) $\tau = 1.5$ fm and (b) $\tau = 4.0$ fm. The two-point correlation function is defined as

$$\langle \delta\tilde{e}(\tau, \eta_s) \delta\tilde{e}(\tau, \eta'_s) \rangle \equiv \frac{\langle \delta e(\tau, \eta_s) \delta e(\tau, \eta'_s) \rangle}{e_0^2(\tau)}, \quad (51)$$

where angular bracket $\langle \dots \rangle$ means both event average and η_s average.⁶ Regarding the structure of correlations itself, correlations grow up around the origin $\Delta\eta_s \approx 0$ and a dip appears at $\Delta\eta_s \approx 0.5$. This is plausible from a viewpoint of the conservation law: the energy density at some point has a negative correlation with that in its vicinity due to energy conservation. The acausal scenario can be demonstrated by taking the $\tau_\pi \rightarrow 0$ limit in Eqs. (28) and (29). We obviously see a difference among the three different settings of the relaxation time at the early stage, $\tau = 1.5$ fm: the correlation with smaller relaxation time of shear pressure tends to propagate faster in the space-time rapidity direction and correlation

⁶The boost invariant property of background enables us to take the average with respect to space-time rapidity, η_s . Throughout the present paper, all correlations are averaged over 10 000 events.

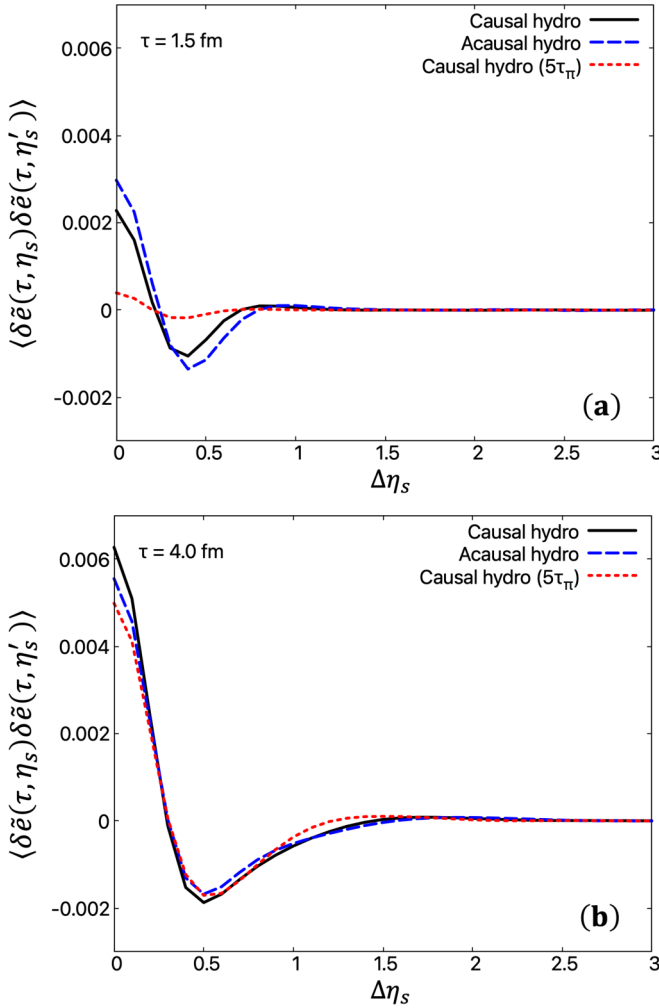


FIG. 5. Normalized correlations of energy density fluctuations as functions of $\Delta \eta_s \equiv |\eta_s - \eta'_s|$. We make a comparison between causal hydro (default settings, black solid line), acausal hydro ($\tau_\pi = 0$ fm, blue dashed line), and causal hydro ($5\tau_\pi$, red dotted line) at (a) $\tau = 1.5$ fm and (b) $\tau = 4.0$ fm.

around the origin becomes stronger. However, the difference becomes tiny at the late stage, $\tau = 4.0$ fm: it takes a longer time to catch up to the final shape of the correlation due to a longer relaxation time. We also analyze the effect of the shear viscosity on energy density correlations in Fig. 6. Apparently, fluids with larger shear viscosity tend to behave more slowly and the dip structures are smeared.

In Fig. 7, we make a comparison of the correlation between the conformal EoS and the lattice EoS. Although the propagation speed of information should be slightly different due to the difference of sound velocity, $c_s^2 = \partial p_0 / \partial e_0$, only a small difference can be seen in this comparison. In general, the sound velocity of lattice EoS is smaller than that of conformal EoS. Hence, information is likely to remain around the origin at which the correlation becomes stronger. That would be the reason why we observe the difference between these two different EoSs. It is noted that the difference in propagation speed can be seen in Fig. 5, which indicates relaxation

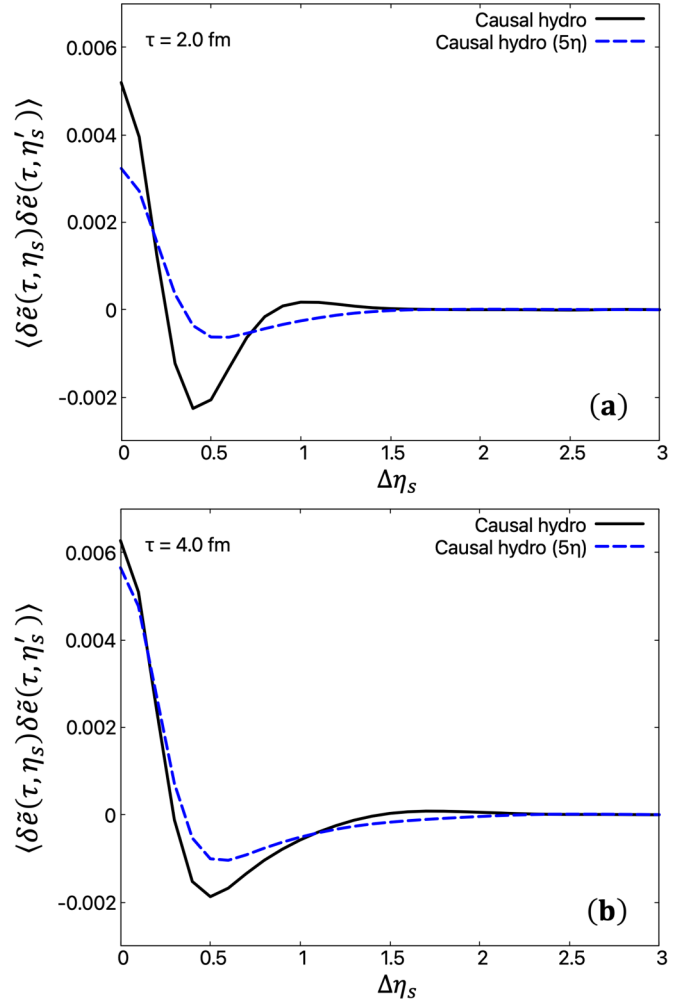


FIG. 6. Normalized correlations of energy density fluctuations as functions of $\Delta \eta_s \equiv |\eta_s - \eta'_s|$. We make a comparison of results from causal hydro with conformal EoS between default settings (black solid line) and 5 times larger η (blue dashed line) at (a) $\tau = 2.0$ fm and (b) $\tau = 4.0$ fm.

time also affects the propagation in the space-time rapidity direction.

We also show correlations of flow rapidity fluctuations in Fig. 8 and shear pressure fluctuations in Fig. 9 as comparisons of the effect of model EoS. The shape of correlations of flow rapidity fluctuations is very similar to that of energy density fluctuations. It is a reasonable behavior as a variable originating from the conservation law of momentum. Note that the difference of propagation speed due to the sound velocity difference is relatively visible at $\tau = 4.0$ fm in Fig. 8: the positions of the second peaks around $\Delta \eta_s \approx 1$ differ. In Fig. 9, we do not observe dips and the second peaks in correlations of fluctuations of shear pressure. The difference in the shape of correlation functions comes from the property of the variable, namely, it is a “fast variable,” which is one of the diffusive quantities and has nothing to do with the conservation law unlike the “slow variables” such as energy density and flow rapidity. The correlations around the origin monotonically grow with time evolution and the magnitude

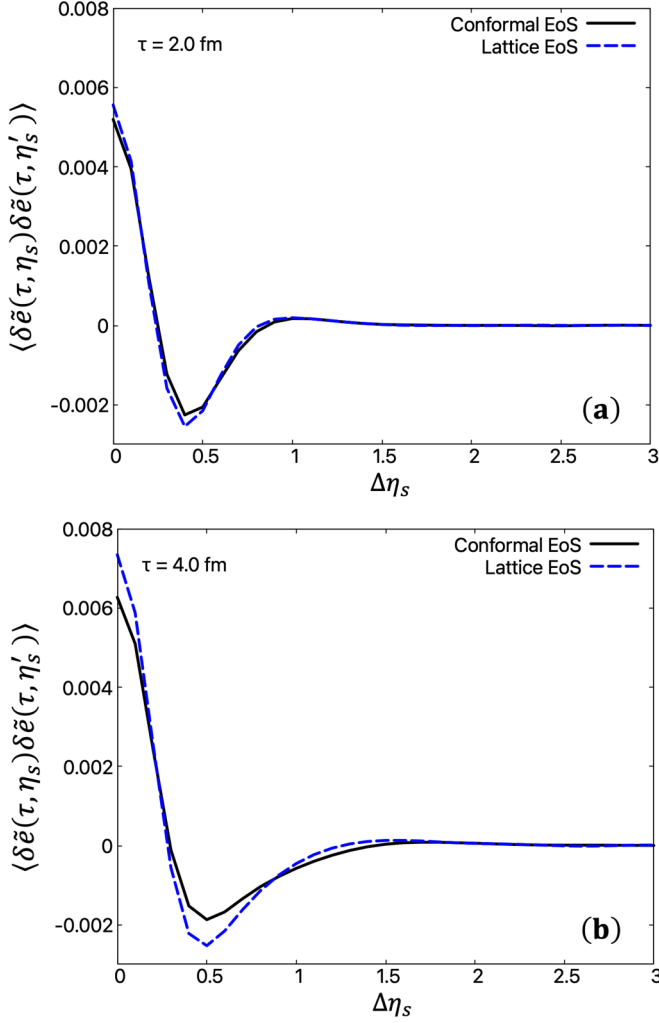


FIG. 7. Normalized correlations of energy density fluctuations as functions of $\Delta\eta_s \equiv |\eta_s - \eta'_s|$. We make a comparison between conformal EoS (default settings, black solid line) and lattice EoS (blue dashed line) at (a) $\tau = 2.0$ fm and (b) $\tau = 4.0$ fm.

is larger in lattice EoS through the whole time evolution. It can be understood from the viewpoint of the FDR. In fact, the shape of shear pressure correlations directly reflects the FDR since the noise term is introduced in the equation of shear pressure fluctuations (29). From the FDR (36), the magnitude of the noises is larger at higher temperature. At a fixed proper time, the background temperature under the expansion with lattice EoS is larger than that with conformal EoS since the sound velocity of the former is in general smaller than that of the latter. Thus, the magnitude of the noises is larger in lattice EoS than in conformal EoS. This behavior has already been discussed [see Eq. (49)] and is also seen in Fig. 1(c) in Sec. III A.

To summarize these results, shear viscosity and relaxation time work to slow down the behaviors of correlations and also suppress the correlations around the origin and propagation in η_s space. Furthermore, the model EoS also affects the behaviors of correlations, which is understood from its sound velocity difference.

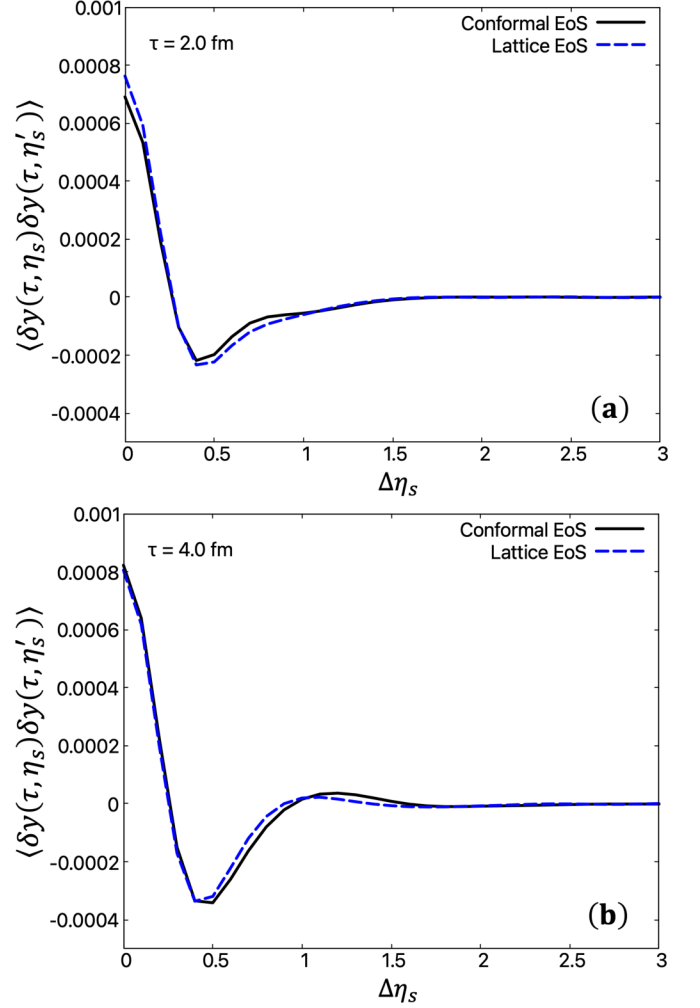


FIG. 8. Correlations of flow rapidity fluctuations as functions of $\Delta\eta_s \equiv |\eta_s - \eta'_s|$. We make a comparison between conformal EoS (default settings, black solid line) and lattice EoS (blue dashed line) at (a) $\tau = 2.0$ fm and (b) $\tau = 4.0$ fm.

D. Two-particle correlation functions

We have analyzed so far the space-time evolution of thermodynamic variables and their correlations. We cannot, however, observe them directly in relativistic heavy ion collision experiments. Therefore it is indispensable to connect these results with experimental observables. To realize this, we calculate momentum distributions of hadrons using the Cooper-Frye formula [52],

$$E \frac{dN}{d^3p} = \frac{d}{(2\pi)^3} \int_{\Sigma(x)} p^\mu d\sigma_\mu(x) f(p^\nu u_\nu(x), T(x)), \quad (52)$$

where d , $p^\mu = (E, \mathbf{p})$, $d\sigma_\mu(x)$, $\Sigma(x)$, and $f(E, T)$ are degeneracy of a hadron under consideration, four-momentum, normal vector of hypersurface element, particleization hypersurface, and one-particle distribution function, respectively. Since we consider finite viscosity, viscous correction to the distribution function should be taken into account [53,54]. Thus, we divide the one-particle distribution function into an

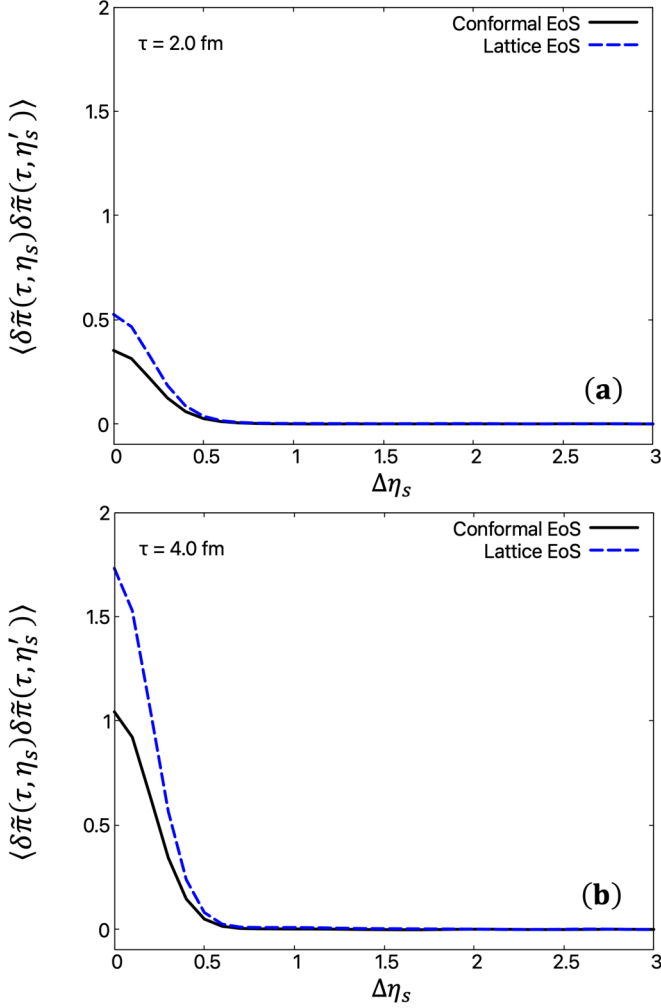


FIG. 9. Normalized correlations of shear pressure fluctuations as functions of $\Delta\eta_s \equiv |\eta_s - \eta'_s|$. We make a comparison between conformal EoS (default settings, black solid line) and lattice EoS (blue dashed line) at (a) $\tau = 2.0$ fm and (b) $\tau = 4.0$ fm.

equilibrium (ideal) part and a near-equilibrium (viscous) part:

$$f = f_{\text{ideal}} + f_{\text{vis}}. \quad (53)$$

For simplicity, we assume Boltzmann distribution for an equilibrium part f_{ideal} and, within our framework, it is written as

$$f_{\text{ideal}}(p_T, Y; \tau, \eta_s) = \exp\left[-\frac{m_T \cosh[Y - \eta_s - \delta y(\tau, \eta_s)]}{T_0(\tau) + \delta T(\tau, \eta_s)}\right], \quad (54)$$

where $Y \equiv \tanh^{-1}(p_z/E)$, $m_T \equiv \sqrt{p_T^2 + m^2}$, T_0 , and δT are rapidity of particles, transverse mass, temperature of background, and fluctuation of temperature, respectively.⁷ On the

⁷Temperature of background, T_0 , and fluctuation of temperature, δT , are calculated from e_0 and δe for a given EoS.

other hand, a near-equilibrium part [54] is written as

$$\begin{aligned} f_{\text{vis}}(p_T, Y; \tau, \eta_s) &= \frac{1}{2sT^3} f_{\text{ideal}} p^\mu p^\nu \pi_{\mu\nu} \\ &= \frac{1}{2(s_0 + \delta s)(T_0 + \delta T)^3} f_{\text{ideal}} \\ &\quad \times \left[\frac{1}{2} p_T^2 - m_T^2 \sinh^2(Y - \eta_s - \delta y) \right] (\pi_0 + \delta\pi), \end{aligned} \quad (55)$$

where s is entropy density and s_0 and δs are its background and fluctuation, respectively. Furthermore, we consider perturbative expansion of f_{ideal} and f_{vis} with respect to the fluctuations δy , δT , δs , and $\delta\pi$ up to the first order following the same prescription as derivation of EoMs of fluctuations in Sec. II. The resultant distributions are

$$\begin{aligned} f_{\text{ideal}} &\approx e^{-\frac{m_T \cosh(Y - \eta_s)}{T_0}} \\ &\quad + e^{-\frac{m_T \cosh(Y - \eta_s)}{T_0}} \left[\frac{m_T \sinh(Y - \eta_s)}{T_0} \delta y \right. \\ &\quad \left. + \frac{m_T \cosh(Y - \eta_s)}{T_0^2} \delta T \right] \\ &\equiv f_{\text{ideal},0} + \delta f_{\text{ideal}}, \end{aligned} \quad (56)$$

where $f_{\text{ideal},0}$ and δf_{ideal} are the zeroth- and the first-order perturbative terms of an equilibrium part, respectively. The perturbative expansion of near-equilibrium parts leads to a much more complicated form:

$$\begin{aligned} f_{\text{vis}} &\approx e^{-\frac{m_T \cosh(Y - \eta_s)}{T_0}} \frac{1}{2s_0 T_0^3} \left[\frac{1}{2} p_T^2 - m_T^2 \sinh^2(Y - \eta_s) \right] \pi_0 \\ &\quad + e^{-\frac{m_T \cosh(Y - \eta_s)}{T_0}} \frac{1}{2s_0 T_0^3} \\ &\quad \times \left\{ \left[\frac{m_T \sinh(Y - \eta_s)}{T_0} \delta y + \frac{m_T \cosh(Y - \eta_s)}{T_0^2} \delta T \right] \right. \\ &\quad \times \left[\frac{1}{2} p_T^2 - m_T^2 \sinh^2(Y - \eta_s) \right] \pi_0 \\ &\quad - \frac{1}{T_0} \left(\frac{1}{c_s^2} + 3 \right) \left[\frac{1}{2} p_T^2 - m_T^2 \sinh^2(Y - \eta_s) \right] \pi_0 \delta T \\ &\quad + 2m_T^2 \sinh(Y - \eta_s) \cosh(Y - \eta_s) \pi_0 \delta y \\ &\quad \left. + \left[\frac{1}{2} p_T^2 - m_T^2 \sinh^2(Y - \eta_s) \right] \delta\pi \right\} \\ &\equiv f_{\text{vis},0} + \delta f_{\text{vis}}, \end{aligned} \quad (57)$$

where $f_{\text{vis},0}$ and δf_{vis} are the zeroth- and the first-order perturbative terms of a near-equilibrium part, respectively. To summarize, we have

$$f = f_{\text{ideal}} + f_{\text{vis}} = f_{\text{ideal},0} + \delta f_{\text{ideal}} + f_{\text{vis},0} + \delta f_{\text{vis}} \quad (58)$$

as a one-particle distribution function to calculate momentum distributions via the Cooper-Frye formula (52).

Rapidity distribution of hadrons is obtained by using the relations $d^3p/E = d^2p_T dY = p_T dp_T dY d\phi = m_T dm_T dY d\phi$,

and by integrating over azimuthal angle:

$$\frac{dN}{dY} = \frac{d}{(2\pi)^2} \tau A \int_{-\infty}^{\infty} d\eta_s \int_m^{\infty} dm_T m_T^2 \cosh(Y - \eta_s) f, \quad (59)$$

where A and m are transverse area and mass of a hadron under consideration, respectively. In the above calculation,

$$\begin{aligned} \left\langle \frac{dN}{dY} \right\rangle &= \frac{d}{(2\pi)^2} \tau A \int_{Y-\Delta\eta'_s}^{Y+\Delta\eta'_s} d\eta_s \cosh(Y - \eta_s) e^{-\frac{m \cosh(Y-\eta_s)}{T_0}} \left\{ \left(1 - \frac{1}{2s_0 T_0^3} m^2 \pi_0 \right) \right. \\ &\times \left[\frac{T_0 m^2}{\cosh(Y - \eta_s)} + \frac{2T_0^2 m}{\cosh^2(Y - \eta_s)} + \frac{2T_0^3}{\cosh^3(Y - \eta_s)} \right] + \frac{1}{2s_0 T_0^3} \left(\frac{1}{2} - \sinh^2(Y - \eta_s) \right) \pi_0 \\ &\times \left. \left[\frac{T_0 m^4}{\cosh(Y - \eta_s)} + \frac{4T_0^2 m^3}{\cosh^2(Y - \eta_s)} + \frac{12T_0^3 m^2}{\cosh^3(Y - \eta_s)} + \frac{24T_0^4 m}{\cosh^4(Y - \eta_s)} + \frac{24T_0^5}{\cosh^5(Y - \eta_s)} \right] \right\}. \quad (60) \end{aligned}$$

Practically, we replaced the integral range of η_s , $[-\infty, \infty]$, with $[Y - \Delta\eta'_s, Y + \Delta\eta'_s]$ since, for a given Y , a contribution from a fluid element being far away from the one at $\eta_s = Y$ can be negligible. We set $\Delta\eta'_s = 3$ in our calculations and confirmed that this range is sufficient enough to converge the integral. The first-order terms, δf_{ideal} and δf_{vis} , do not contribute to the final one-particle momentum distribution due to $\langle \delta f \rangle = 0$. It is noted that, in the derivation of Eq. (60), an integral with respect to transverse mass is analytically solved using the incomplete gamma function (see also Appendix B).

Two-particle correlation functions in the rapidity direction, $\langle \frac{dN}{dY_1} \frac{dN}{dY_2} \rangle$, are also obtained from the Cooper-Frye formula (52) after straightforward but lengthy calculations.⁸ Here subscripts 1 and 2 are labels of particles 1 and 2, respectively. See also Appendix B for details of two-particle correlation functions. Finally, we obtain the normalized two-particle correlations $\langle \frac{dN}{dY_1} \frac{dN}{dY_2} \rangle / \langle \frac{dN}{dY_1} \rangle \langle \frac{dN}{dY_2} \rangle$ as a function of rapidity gap $\Delta Y \equiv |Y_1 - Y_2|$. In what follows, the default model of the EoS is the lattice EoS although we employ the conformal EoS for the sake of comparison.⁹

Figure 10 shows the normalized two-particle correlation functions as functions of rapidity gap ΔY for massless particles ($m = 0$ GeV), charged pions ($m = 0.139$ GeV), charged kaons ($m = 0.494$ GeV), and protons ($m = 0.938$ GeV) without any contributions from resonance decays. Lattice EoS and default setting for transport coefficients are employed to describe the hydrodynamic evolution in this analysis. We assume that all hadrons freeze out at $\tau = 10.0$ fm which corresponds to freeze-out temperature $T \simeq 0.168$ GeV in the lattice EoS and transport coefficients employed in this study.

⁸Here we neglect possible quantum correlations between two identical particles.

⁹In the conformal EoS, the constituents of the fluids should be massless particles. Nevertheless, we employ it and calculate spectra for massive particles to capture the difference in hydrodynamic evolution between conformal EoS and lattice EoS.

we assumed isochronous freeze-out at τ and also used the relation $p^\mu d\sigma_\mu = \tau A d\eta_s m_T \cosh(Y - \eta_s)$ by neglecting possible small changes of freeze-out hypersurface due to fluctuations. By taking an average of Eq. (59) over events and integrating over m_T , the first-order perturbative parts in the one-particle distribution function vanish. We finally obtain

Since the two-particle correlation functions have a value rather than unity when two-point correlation functions such as $\langle \delta T(\eta_{s1}) \delta T(\eta_{s2}) \rangle$ and $\langle \delta y(\eta_{s1}) \delta y(\eta_{s2}) \rangle$ are finite, it is obvious that the information at freeze-out is inherited by two-particle correlation functions. Moreover, the pattern of the correlations is more clearly seen for heavier hadrons. It indicates that the heavier hadrons are good probes of correlations and that they can be used to extract the properties of the expanding media. As one sees, positions and depths (heights) of dips (bumps) of correlations depend on the mass of hadrons. One can interpret this behavior from the viewpoint of thermal fluctuations. The ratio m/T_0 appearing in Eq. (60) is a good measure of thermal fluctuations in a fluid element and characterizes the shape of correlations: the momentum rapidity, Y , of heavier hadrons

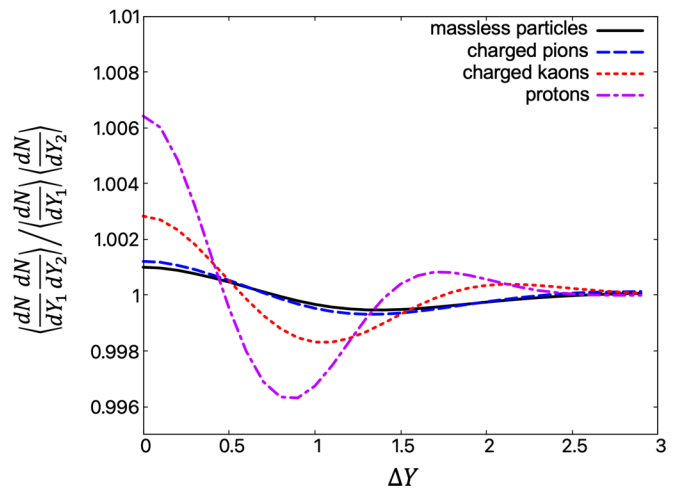


FIG. 10. Normalized two-particle correlation functions as functions of $\Delta Y \equiv |Y_1 - Y_2|$ for massless particles (black solid line), charged pions (blue dashed line), charged kaons (red dotted line), and protons (magenta dash-dotted line) at freeze-out time $\tau = 10.0$ fm and the corresponding background temperature $T_0 \simeq 0.168$ GeV. Lattice EoS is employed for hydrodynamic evolution.

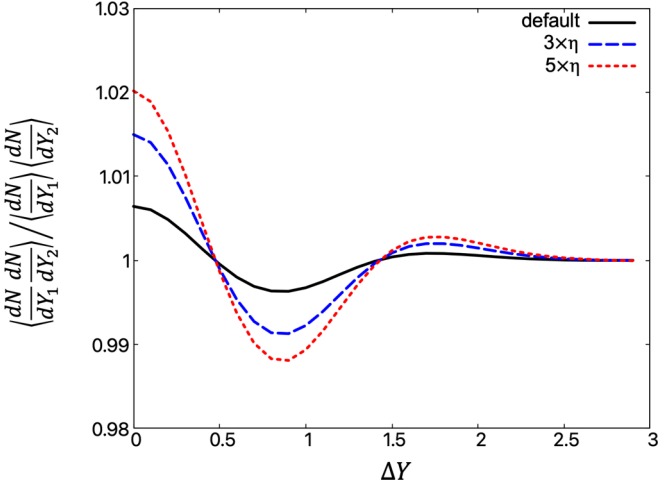


FIG. 11. Normalized two-particle correlation functions of protons as functions of $\Delta Y \equiv |Y_1 - Y_2|$ for default set of shear viscosity η (black solid line), 3 times larger η (blue dashed line), and 5 times larger η (red dotted line) at freeze-out time $\tau = 10.0$ fm. Lattice EoS and the default relaxation time are employed for hydrodynamic evolution.

tends to reflect the flow rapidity, y_f , at freeze-out, namely $Y \approx y_f$, while the pattern that correlations of thermodynamic variables possess in the space-time rapidity is blurred by thermal fluctuations in the correlations of lighter particles in momentum rapidity space.

In Figs. 11 and 12, we elucidate how the two-particle correlation functions of protons depend on the transport coefficients under the space-time evolution with lattice EoS. The correlation pattern becomes more visible by increasing shear viscosity as shown in Fig. 11. On the other hand, the magnitude decreases with increasing relaxation time as shown in

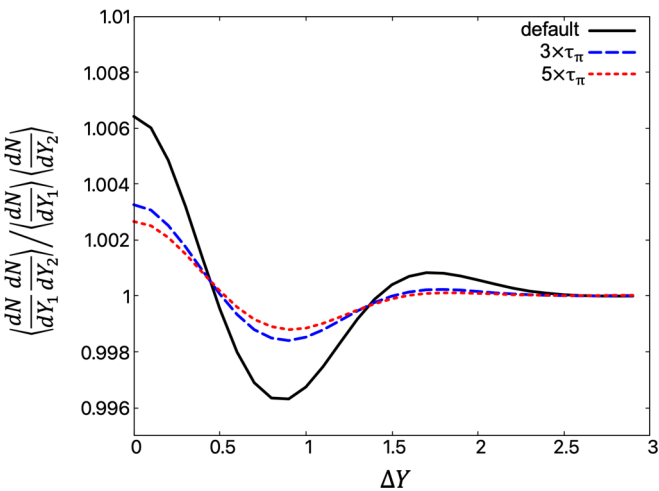


FIG. 12. Normalized two-particle correlation functions of protons as functions of $\Delta Y \equiv |Y_1 - Y_2|$ for default set of relaxation time τ_π (black solid line), 3 times larger τ_π (blue dashed line), and 5 times larger τ_π (red dotted line) at freeze-out time $\tau = 10.0$ fm. Lattice EoS and the default shear viscosity are employed for hydrodynamic evolution.

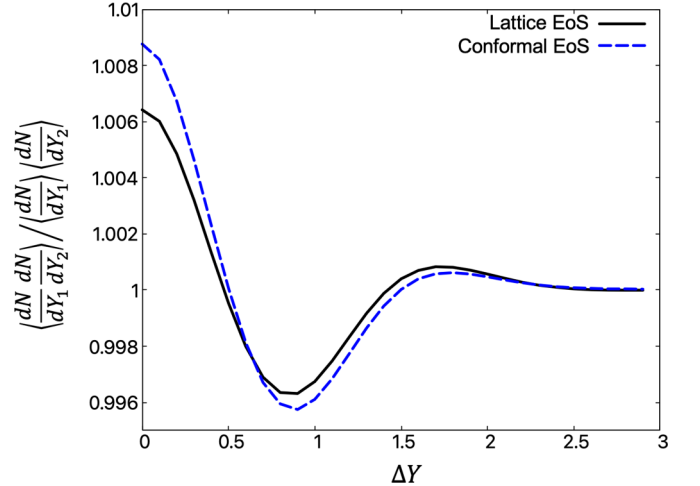


FIG. 13. Normalized two-particle correlations of protons as functions of $\Delta Y \equiv |Y_1 - Y_2|$. We make a comparison of the results between lattice EoS (black solid line) and conformal EoS (blue dashed line) at $T_0 \simeq 0.168$ GeV. Regarding the difference in freeze-out time, see the text.

Fig. 12. The magnitude of two-particle correlation functions turns out to be highly sensitive to the transport properties of the media although positions of dips and bumps of the two-particle correlations do not depend on the choice of shear viscosity and relaxation time within a certain range. This clearly exhibits that the two-particle correlation functions of relatively heavy hadrons open up a new window to study the transport properties of the media created in relativistic heavy ion collisions.

In Fig. 13, we make a comparison of the proton two-particle correlation functions between conformal EoS and lattice EoS. When we analyze the correlation functions of energy density fluctuations, the magnitude of lattice EoS is larger than that of conformal EoS as shown in Fig. 7. However, this behavior is opposite in the two-particle correlation functions of protons: the magnitude of two-particle correlation functions of protons with conformal EoS is larger than that of lattice EoS. This is due to the difference in freeze-out time. In fact, fluids with conformal EoS reach $T_0 \simeq 0.168$ GeV faster than the ones with lattice EoS. Thus, freeze-out time depends on the choice of the model EoS: $\tau = 4.3$ fm for conformal EoS with the degree of freedom $d = 47.5$, and $\tau = 10.0$ fm for lattice EoS. Thus two-particle correlation functions with conformal EoS reflect the early time correlations of thermodynamic variables which are in the course of growing rapidly.

IV. SUMMARY

In this paper, we developed a framework which deals with causal hydrodynamic fluctuations in a one-dimensional expanding system. Since the EoS are derived without any assumption of specific constitutive equations, one employs any kinds of constitutive equations proposed so far for shear pressure π and bulk pressure Π . In the present work, we employed the simplest second-order constitutive equations derived by Israel and Stewart which satisfy the causality. We

solved a system of stochastic partial differential equations and analyzed the dynamics of (1+1)-dimensional causal hydrodynamic fluctuations on an event-by-event basis. Through the description of space-time evolution of thermodynamic variables, we found a novel phenomenon, an almost frozen structure of energy density fluctuations and flow rapidity fluctuations. From the analysis of the structure, it could be possible to extract information of the early stage of hydrodynamic evolution, such as thermal fluctuations. We also investigated the two-point correlation functions of energy density fluctuations which are induced by hydrodynamic fluctuations and saw the dependence on various settings of the bulk and the transport properties. The correlations are sensitive to the settings of EoS and transport coefficients such as relaxation time and viscosity. To extract properties of the media in comparison with experimental data, it is also important to analyze the effects of correlations of thermodynamic variables on two-particle correlation functions which are observables in experiments. Utilizing the Cooper-Frye formula, we analytically derived the specific form of two-particle correlation functions including two-point correlation functions of thermodynamic variables, flow rapidity, shear pressure, and cross-terms among them. We show that the two-point correlations of these hydrodynamic variables are inherited by two-particle correlations in the final state. We found that correlations are more enhanced for heavier particles. It indicates that heavier hadrons are good probes to see the consequences of hydrodynamic fluctuations. We also show that the two-particle correlation functions are sensitive to the properties of the medium. Specifically, the correlations enhance with increasing shear viscosity or decreasing relaxation time. Sound velocity also affects the shape of correlations, therefore we have a chance to extract the information of the EoS through analysis of the two-particle correlation functions. These results provide us with an opportunity for multidimensional analysis of properties of the QGP created in relativistic heavy ion collisions.

In the present paper, we assumed one of the simplest settings, e.g., the simplest one-dimensional expanding system, the simplest EoS, the simplest causal constitutive equations, and we neglect charge current and bulk pressure. Therefore, there is a lot of room for sophistication and extension. As one way of major extension, the (3+1)-dimensional expanding analytic solution [23], instead of the one-dimensional boost invariant solution (2), could be employed by following the same prescription that we explained in this paper. Regarding the FDRs (33) and (35), it is known that these FDRs need additional correction terms when the background system is nonstatic and constitutive equations have finite relaxation effects [47]. It would be intriguing to see the effects of expansion and finite relaxation on the two-point correlations of hydrodynamic variables. Including fluctuations of conserved charges [55–57] in the present framework might be also interesting. Through the description of causal propagation and diffusion of charge fluctuations, we may have a chance to extract the diffusion coefficients of conserved charges. Since it is beyond the scope of the present study, we leave it for future work.

The present framework can be utilized to search for the critical point of the QCD phase diagram through the analysis of detailed dynamics of both hydrodynamic and critical fluctuations. Fluctuations of the order parameter of chiral phase transition in the vicinity of the critical point are “fast modes,” therefore such information is likely to be lost due to the diffusive mode in the QGP. The fluctuations of the order parameter are, however, taken over by the “slow modes,” namely, fluctuations of baryon number density [58,59]. Chasing the dynamics of both the slow modes and the fast mode [60], we can diagnose the QCD phase diagram and have a chance to pin down the location of the critical point, but we leave it for future study.

ACKNOWLEDGMENTS

We would like to thank C. Chattopadhyay for giving us some useful references. We also thank S. Jeon for giving us some valuable comments and Y. Kanakubo and K. Kuroki for fruitful discussions. The work by T.H. was partly supported by JSPS KAKENHI Grant No. JP19K21881.

APPENDIX A: SOUND PROPAGATION

Here let us discuss the propagation of sound waves (or density fluctuations) in the t - z plane and τ - η_s plane, and show that the behavior is completely different if the background medium expands. One can define the effective sound velocity c'_s , in which the tailwind from the expanding system is included, as

$$c'_s(t, z) = \frac{dz(t)}{dt} = \tanh[\eta_s(t, z) + y_s] = \frac{c_s t + z(t)}{t + c_s z(t)}, \quad (\text{A1})$$

where $\eta_s(t, z) = \tanh^{-1}(z/t)$ and $y_s \equiv \tanh^{-1} c_s$, and c_s is a constant sound velocity. By performing a variable transformation $z(t)/t = v(t)$, one solves Eq. (A1) with an initial condition, $z(t = t_0) = z_0$, transforms the solution to τ and η_s , and obtains $\tau/\tau_0 = e^{\Delta\eta_s/c_s}$, where $\Delta\eta_s \equiv |\eta_s(t, z) - \eta_{s0}|$. Here $\tau_0 = \sqrt{t_0^2 - z_0^2}$ and $\eta_{s0} = \eta_s(t_0, z_0)$. On the other hand, propagation of light is described as either $t - t_0 = z - z_0$ in the t - z plane or $\tau/\tau_0 = e^{\Delta\eta_s}$ in the τ - η_s plane. Figure 14 shows the resultant propagation of sounds in (a) the t - z plane and (b) the τ - η_s plane with sound velocity $c_s = 1/\sqrt{3}$ and specific initial conditions. In contrast to the case without tailwind, the slope of the propagation with tailwind approaches that of light cone asymptotically in t - z plane. In other words, the propagation speed of sound approaches the speed of light in the long time limit even though the initial sound velocity is $c_s = 1/\sqrt{3}$ due to the expansion of the system. Moreover, propagation of sounds goes to infinity in η_s space in this case. On the other hand, there is a singularity at $\eta_s = y_s = \tanh^{-1}(1/\sqrt{3}) \simeq 0.66$ in the τ - η_s plane in the case without tailwind. This is the so-called sound horizon.

APPENDIX B: TWO-PARTICLE CORRELATION FUNCTIONS

We obtain the event-averaged two-particle correlation function as a function of rapidity gap after inserting the

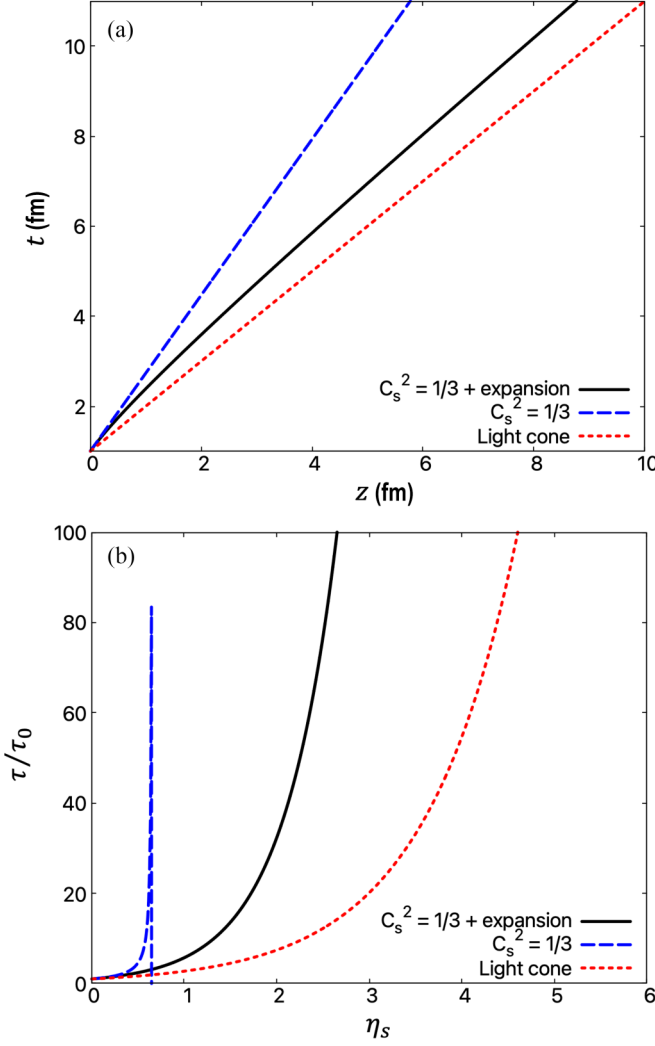


FIG. 14. Sound propagation in (a) the t - z plane with an initial condition ($t_0 = 1$ fm and $z_0 = 0$ fm) and in (b) the τ - η_s plane with an initial condition ($\tau_0 = t_0$ and $\eta_{s0} = \eta_s(t_0, 0) = 0$). The black solid line, blue dashed line, and red dotted line denote propagation with tailwind, that without tailwind, and light cone, respectively. Sound velocity $c_s = 1/\sqrt{3}$ is assumed.

explicit forms of distribution functions (56) and (57) into the following form:

$$\begin{aligned}
 \left\langle \frac{dN}{dY_1} \frac{dN}{dY_2} \right\rangle &= \left[\frac{d\tau A}{(2\pi)^2} \right]^2 \int_{Y_1 - \Delta\eta'_{s1}}^{Y_1 + \Delta\eta'_{s1}} d\eta_{s1} \int_{Y_2 - \Delta\eta'_{s2}}^{Y_2 + \Delta\eta'_{s2}} d\eta_{s2} \\
 &\times \int_m^\infty dm_{T1} \int_m^\infty dm_{T2} m_{T1}^2 m_{T2}^2 \\
 &\times \cosh(Y_1 - \eta_{s1}) \cosh(Y_2 - \eta_{s2}) \\
 &\times \langle (f_{\text{ideal},0}^{(1)} f_{\text{ideal},0}^{(2)} + 2f_{\text{ideal},0}^{(1)} f_{\text{vis},0}^{(2)} + f_{\text{vis},0}^{(1)} f_{\text{vis},0}^{(2)} \\
 &+ \delta f_{\text{ideal}}^{(1)} \delta f_{\text{ideal}}^{(2)} + 2\delta f_{\text{ideal}}^{(1)} \delta f_{\text{vis}}^{(2)} + \delta f_{\text{vis}}^{(1)} \delta f_{\text{vis}}^{(2)}) \rangle.
 \end{aligned} \tag{B1}$$

Here upper indices 1 and 2 in the distribution functions denote variables of particles 1 and 2, respectively. Terms including single δf_{ideal} or δf_{vis} are neglected since they do not contribute to the final results due to $\langle \delta f \rangle = 0$. The next step is to integrate Eq. (B1) over m_{T1} and m_{T2} . Since the resultant form of two-particle correlation functions is significantly complicated, we introduce new variables as follows to avoid the complexity:

$$A_{1/2}(n) \equiv \sum_{i=0}^n \frac{T_0^{i+1} P(n, i) m_{T1/2}^{n-i}}{\cosh^{i+1}(Y_{1/2} - \eta_{s1/2})}, \tag{B2}$$

$$B \equiv \frac{1}{2s_0 T_0^3}, \tag{B3}$$

$$C_{1/2} \equiv \frac{1}{2} - \sinh^2(Y_{1/2} - \eta_{s1/2}), \tag{B4}$$

$$D \equiv \frac{1}{2} m^2, \tag{B5}$$

$$E \equiv \frac{1}{2s_0 T_0} \left(\frac{1}{c_s^2} + 3 \right), \tag{B6}$$

$$F_{1/2} \equiv 2 \sinh(Y_{1/2} - \eta_{s1/2}) \cosh(Y_{1/2} - \eta_{s1/2}), \tag{B7}$$

$$\begin{aligned}
 G_{12} &\equiv \frac{\cosh(Y_1 - \eta_{s1}) \cosh(Y_2 - \eta_{s2})}{T_0^4} \delta T(\eta_{s1}) \delta T(\eta_{s2}) \\
 &+ \frac{\sinh(Y_1 - \eta_{s1}) \cosh(Y_2 - \eta_{s2})}{T_0^3} \delta y(\eta_{s1}) \delta T(\eta_{s2}) \\
 &+ \frac{\cosh(Y_1 - \eta_{s1}) \sinh(Y_2 - \eta_{s2})}{T_0^3} \delta T(\eta_{s1}) \delta y(\eta_{s2}) \\
 &+ \frac{\sinh(Y_1 - \eta_{s1}) \sinh(Y_2 - \eta_{s2})}{T_0^2} \delta y(\eta_{s1}) \delta y(\eta_{s2}).
 \end{aligned} \tag{B8}$$

Here the index “1/2” denotes either particle 1 or particle 2. A coefficient of the incomplete gamma function, $A_{1/2}(n)$, is defined as

$$\begin{aligned}
 &\int_m^\infty dm_{T1/2} m_{T1/2}^n e^{-\frac{m_{T1/2} \cosh(Y_{1/2} - \eta_{s1/2})}{T_0}} \\
 &= \sum_{i=0}^n \frac{T_0^{i+1} P(n, i) m_{T1/2}^{n-i}}{\cosh^{i+1}(Y_{1/2} - \eta_{s1/2})} e^{-\frac{m \cosh(Y_{1/2} - \eta_{s1/2})}{T_0}} \\
 &= A_{1/2}(n) e^{-\frac{m \cosh(Y_{1/2} - \eta_{s1/2})}{T_0}},
 \end{aligned} \tag{B9}$$

where the permutation is calculated as $P(n, i) = n!/(n - i)!$. Using these variables, the resultant two-particle correlation leads to

$$\left\langle \frac{dN}{dY_1} \frac{dN}{dY_2} \right\rangle = \left[\frac{d\tau A}{(2\pi)^2} \right]^2 \int_{Y_1 - \Delta\eta'_{s1}}^{Y_1 + \Delta\eta'_{s1}} d\eta_{s1} \int_{Y_2 - \Delta\eta'_{s2}}^{Y_2 + \Delta\eta'_{s2}} d\eta_{s2} \cosh(Y_1 - \eta_{s1}) \cosh(Y_2 - \eta_{s2}) \times \langle ((\text{I}) + 2 \times (\text{II}) + (\text{III}) + (\text{IV}) + 2 \times (\text{V}) + (\text{VI})) \rangle, \quad (\text{B10})$$

$$(\text{I}) = \int_m^\infty dm_{T1} \int_m^\infty dm_{T2} m_{T1}^2 m_{T2}^2 f_{\text{ideal},0}^{(1)} f_{\text{ideal},0}^{(2)} = A_1(2)A_2(2)e^{-\frac{m[\cosh(Y_1 - \eta_{s1}) + \cosh(Y_2 - \eta_{s2})]}{T_0}}, \quad (\text{B11})$$

$$(\text{II}) = \int_m^\infty dm_{T1} \int_m^\infty dm_{T2} m_{T1}^2 m_{T2}^2 f_{\text{ideal},0}^{(1)} f_{\text{vis},0}^{(2)} = [A_1(2)A_2(4)BC_2\pi_0 - A_1(2)A_2(2)BD\pi_0]e^{-\frac{m[\cosh(Y_1 - \eta_{s1}) + \cosh(Y_2 - \eta_{s2})]}{T_0}}, \quad (\text{B12})$$

$$(\text{III}) = \int_m^\infty dm_{T1} \int_m^\infty dm_{T2} m_{T1}^2 m_{T2}^2 f_{\text{vis},0}^{(1)} f_{\text{vis},0}^{(2)} = [A_1(4)A_2(4)B^2C_1C_2\pi_0^2 - A_1(4)A_2(2)B^2C_1D\pi_0^2 - A_1(2)A_2(4)B^2C_2D\pi_0^2 + A_1(2)A_2(2)B^2D^2\pi_0^2]e^{-\frac{m[\cosh(Y_1 - \eta_{s1}) + \cosh(Y_2 - \eta_{s2})]}{T_0}}, \quad (\text{B13})$$

$$(\text{IV}) = \int_m^\infty dm_{T1} \int_m^\infty dm_{T2} m_{T1}^2 m_{T2}^2 \delta f_{\text{ideal}}^{(1)} \delta f_{\text{ideal}}^{(2)} = A_1(3)A_2(3)G_{12}e^{-\frac{m[\cosh(Y_1 - \eta_{s1}) + \cosh(Y_2 - \eta_{s2})]}{T_0}}, \quad (\text{B14})$$

$$(\text{V}) = \int_m^\infty dm_{T1} \int_m^\infty dm_{T2} m_{T1}^2 m_{T2}^2 \delta f_{\text{ideal}}^{(1)} \delta f_{\text{vis}}^{(2)} = \left\{ A_1(3)A_2(5)G_{12}BC_2\pi_0 - A_1(3)A_2(3)G_{12}BD\pi_0 - A_1(3)A_2(4)EC_2\pi_0 \right. \\ \times \left[\frac{\sinh(Y_1 - \eta_{s1})}{T_0} \delta y(\eta_{s1}) \delta T(\eta_{s2}) + \frac{\cosh(Y_1 - \eta_{s1})}{T_0^2} \delta T(\eta_{s1}) \delta T(\eta_{s2}) \right] + A_1(3)A_2(4)BF_2\pi_0 \\ \times \left[\frac{\sinh(Y_1 - \eta_{s1})}{T_0} \delta y(\eta_{s1}) \delta y(\eta_{s2}) + \frac{\cosh(Y_1 - \eta_{s1})}{T_0^2} \delta T(\eta_{s1}) \delta y(\eta_{s2}) \right] + A_1(3)A_2(4)BC_2 \\ \times \left[\frac{\sinh(Y_1 - \eta_{s1})}{T_0} \delta y(\eta_{s1}) \delta \pi(\eta_{s2}) + \frac{\cosh(Y_1 - \eta_{s1})}{T_0^2} \delta T(\eta_{s1}) \delta \pi(\eta_{s2}) \right] + A_1(3)A_2(2)ED\pi_0 \\ \times \left[\frac{\sinh(Y_1 - \eta_{s1})}{T_0} \delta y(\eta_{s1}) \delta T(\eta_{s2}) + \frac{\cosh(Y_1 - \eta_{s1})}{T_0^2} \delta T(\eta_{s1}) \delta T(\eta_{s2}) \right] - A_1(3)A_2(2)BD \\ \times \left. \left[\frac{\sinh(Y_1 - \eta_{s1})}{T_0} \delta y(\eta_{s1}) \delta \pi(\eta_{s2}) + \frac{\cosh(Y_1 - \eta_{s1})}{T_0^2} \delta T(\eta_{s1}) \delta \pi(\eta_{s2}) \right] \right\} e^{-\frac{m[\cosh(Y_1 - \eta_{s1}) + \cosh(Y_2 - \eta_{s2})]}{T_0}}, \quad (\text{B15})$$

$$(\text{VI}) = \int_m^\infty dm_{T1} \int_m^\infty dm_{T2} m_{T1}^2 m_{T2}^2 \delta f_{\text{vis}}^{(1)} \delta f_{\text{vis}}^{(2)} = \left(\{ A_1(5)A_2(5)G_{12}B^2C_1C_2\pi_0^2 - A_1(5)A_2(3)G_{12}B^2C_1D\pi_0^2 \right. \\ - A_1(3)A_2(5)G_{12}B^2C_2D\pi_0^2 + A_1(3)A_2(3)G_{12}B^2D^2\pi_0^2 + [A_1(4)A_2(4)E^2C_1C_2\pi_0^2 - A_1(4)A_2(2)E^2C_1D\pi_0^2 \\ - A_1(2)A_2(4)E^2C_2D\pi_0^2 + A_1(2)A_2(2)E^2D^2\pi_0^2] \delta T(\eta_{s1}) \delta T(\eta_{s2}) + A_1(4)A_2(4)B^2F_1F_2\pi_0^2 \delta y(\eta_{s1}) \delta y(\eta_{s2}) \\ + [A_1(4)A_2(4)B^2C_1C_2 - A_1(4)A_2(2)B^2C_1D - A_1(2)A_2(4)B^2C_2D + A_1(2)A_2(2)B^2D^2] \delta \pi(\eta_{s1}) \delta \pi(\eta_{s2}) \} \\ + 2 \left\{ [-A_1(5)A_2(4)BEC_1C_2\pi_0^2 + A_1(3)A_2(4)BEDC_2\pi_0^2 + A_1(5)A_2(2)BEC_1D\pi_0^2 - A_1(3)A_2(2)BED^2\pi_0^2] \right. \\ \times \left[\frac{\sinh(Y_1 - \eta_{s1})}{T_0} \delta y(\eta_{s1}) \delta T(\eta_{s2}) + \frac{\cosh(Y_1 - \eta_{s1})}{T_0^2} \delta T(\eta_{s1}) \delta T(\eta_{s2}) \right] + [A_1(5)A_2(4)B^2C_1F_2\pi_0^2 \\ - A_1(3)A_2(4)B^2DF_2\pi_0^2] \left. \left[\frac{\sinh(Y_1 - \eta_{s1})}{T_0} \delta y(\eta_{s1}) \delta y(\eta_{s2}) + \frac{\cosh(Y_1 - \eta_{s1})}{T_0^2} \delta T(\eta_{s1}) \delta y(\eta_{s2}) \right] \right)$$

$$\begin{aligned}
& + [A_1(5)A_2(4)B^2C_1C_2\pi_0 - A_1(3)A_2(4)B^2DC_2\pi_0 - A_1(5)A_2(2)B^2C_1D\pi_0 + A_1(3)A_2(2)B^2D^2\pi_0] \\
& \times \left[\frac{\sinh(Y_1 - \eta_{s1})}{T_0} \delta y(\eta_{s1}) \delta \pi(\eta_{s2}) + \frac{\cosh(Y_1 - \eta_{s1})}{T_0^2} \delta T(\eta_{s1}) \delta \pi(\eta_{s2}) \right] \\
& + [-A_1(4)A_2(4)BEC_1F_2\pi_0^2 + A_1(2)A_2(4)BEDF_2\pi_0^2] \delta T(\eta_{s1}) \delta y(\eta_{s2}) \\
& + [-A_1(4)A_2(4)BEC_1C_2\pi_0 + A_1(4)A_2(2)BEC_1D\pi_0 + A_1(2)A_2(4)BEC_2D\pi_0 - A_1(2)A_2(2)BED^2\pi_0] \\
& \times \delta T(\eta_{s1}) \delta \pi(\eta_{s2}) + [A_1(4)A_2(4)B^2F_1C_2\pi_0 - A_1(4)A_2(2)B^2F_1D\pi_0] \delta y(\eta_{s1}) \delta \pi(\eta_{s2}) \Big\} e^{-\frac{m[\cosh(Y_1 - \eta_{s1}) + \cosh(Y_2 - \eta_{s2})]}{T_0}}.
\end{aligned} \tag{B16}$$

The terms (IV), (V), and (VI) play a crucial role in reflecting the correlations of thermodynamic variables in the two-particle correlation functions. Performing η_{s1} and η_{s2} integration of (B10) numerically, we finally obtain the two-particle correlation as a function of rapidity gap, $\Delta Y \equiv |Y_1 - Y_2|$.

In Eq. (B10), we considered up to the second order in perturbation (fluctuation) and up to the second order in viscous correction. Orders of each term are summarized in Table II. Strictly speaking, the second-order perturbative terms from the one-particle distribution or the second order viscous corrections should have been considered from an order counting point of view in the form of two-particle correlation (B10), e.g., $f_{\text{ideal},0} \delta^2 f_{\text{vis}}$. However, we neglected such terms since

we expanded the distribution only up to the first order of perturbation and viscous correction as Eq. (58).

TABLE II. Orders of each term.

Term	Perturbation	Viscous correction
$f_{\text{ideal},0} f_{\text{ideal},0}$	0	0
$f_{\text{ideal},0} f_{\text{vis},0}$	0	1
$f_{\text{vis},0} f_{\text{vis},0}$	0	2
$\delta f_{\text{ideal}} \delta f_{\text{ideal}}$	2	0
$\delta f_{\text{ideal}} \delta f_{\text{vis}}$	2	1
$\delta f_{\text{vis}} \delta f_{\text{vis}}$	2	2

- [1] P. F. Kolb, P. Huovinen, U. W. Heinz, and H. Heiselberg, *Phys. Lett. B* **500**, 232 (2001).
- [2] P. Huovinen, P. F. Kolb, U. W. Heinz, P. V. Ruuskanen, and S. A. Voloshin, *Phys. Lett. B* **503**, 58 (2001).
- [3] U. W. Heinz and P. F. Kolb, *Nucl. Phys. A* **702**, 269 (2002).
- [4] D. Teaney, J. Lauret, and E. V. Shuryak, *Phys. Rev. Lett.* **86**, 4783 (2001).
- [5] T. Hirano, *Phys. Rev. C* **65**, 011901(R) (2001).
- [6] T. Hirano and K. Tsuda, *Phys. Rev. C* **66**, 054905 (2002).
- [7] T. Hirano and M. Gyulassy, *Nucl. Phys. A* **769**, 71 (2006).
- [8] J. E. Bernhard, J. S. Moreland, S. A. Bass, J. Liu, and U. Heinz, *Phys. Rev. C* **94**, 024907 (2016).
- [9] J. E. Bernhard, J. S. Moreland, and S. A. Bass, *Nat. Phys.* **15**, 1113 (2019).
- [10] J. Auvinen, K. J. Eskola, P. Huovinen, H. Niemi, R. Paatelainen, and P. Petreczky, *Phys. Rev. C* **102**, 044911 (2020).
- [11] G. Nijs, W. van der Schee, U. Gürsoy, and R. Snellings, *Phys. Rev. Lett.* **126**, 202301 (2021).
- [12] G. Nijs, W. van der Schee, U. Gürsoy, and R. Snellings, *Phys. Rev. C* **103**, 054909 (2021).
- [13] J. E. Parkkila, A. Onnerstad, and D. J. Kim, *Phys. Rev. C* **104**, 054904 (2021).
- [14] D. Everett *et al.* (JETSCAPE Collaboration), *Phys. Rev. C* **103**, 054904 (2021).
- [15] M. R. Heffernan, C. Gale, S. Jeon, and J.-F. Paquet, [arXiv:2306.09619](https://arxiv.org/abs/2306.09619).
- [16] C. Shen, B. Schenke, and W. Zhao, [arXiv:2310.10787](https://arxiv.org/abs/2310.10787).
- [17] R. Kubo, *J. Phys. Soc. Jpn.* **12**, 570 (1957).
- [18] J. D. Bjorken, *Phys. Rev. D* **27**, 140 (1983).
- [19] H. Kouno, M. Maruyama, F. Takagi, and K. Saito, *Phys. Rev. D* **41**, 2903 (1990).
- [20] G. S. Denicol, T. Kodama, T. Koide, and P. Mota, *J. Phys. G* **35**, 115102 (2008).
- [21] J. I. Kapusta, B. Muller, and M. Stephanov, *Phys. Rev. C* **85**, 054906 (2012).
- [22] L. Yan and H. Grönqvist, *J. High Energy Phys.* 03 (2016) 121.
- [23] S. S. Gubser, *Phys. Rev. D* **82**, 085027 (2010).
- [24] W. A. Hiscock and L. Lindblom, *Ann. Phys. (NY)* **151**, 466 (1983).
- [25] W. A. Hiscock and L. Lindblom, *Phys. Rev. D* **31**, 725 (1985).
- [26] W. A. Hiscock and L. Lindblom, *Phys. Rev. D* **35**, 3723 (1987).
- [27] W. Israel, *Ann. Phys. (NY)* **100**, 310 (1976).
- [28] W. Israel and J. M. Stewart, *Ann. Phys. (NY)* **118**, 341 (1979).
- [29] R. Baier, P. Romatschke, and U. A. Wiedemann, *Phys. Rev. C* **73**, 064903 (2006).
- [30] R. Baier, P. Romatschke, D. T. Son, A. O. Starinets, and M. A. Stephanov, *J. High Energy Phys.* 04 (2008) 100.
- [31] B. Betz, D. Henkel, and D. H. Rischke, *Prog. Part. Nucl. Phys.* **62**, 556 (2009).
- [32] B. Betz, D. Henkel, and D. H. Rischke, *J. Phys. G* **36**, 064029 (2009).
- [33] G. S. Denicol, H. Niemi, E. Molnar, and D. H. Rischke, *Phys. Rev. D* **85**, 114047 (2012); **91**, 039902(E) (2015).
- [34] A. Monnai and T. Hirano, *Nucl. Phys. A* **847**, 283 (2010).
- [35] A. Jaiswal, R. S. Bhalerao, and S. Pal, *Phys. Rev. C* **87**, 021901(R) (2013).
- [36] A. Jaiswal, *Phys. Rev. C* **87**, 051901(R) (2013).
- [37] K. Tsumura, Y. Kikuchi, and T. Kunihiro, *Phys. Rev. D* **92**, 085048 (2015).

- [38] C. Chattopadhyay, R. S. Bhalerao, and S. Pal, *Phys. Rev. C* **97**, 054902 (2018).
- [39] K. Murase, Causal hydrodynamic fluctuations and their effects on high-energy nuclear collisions, Ph.D. thesis, Tokyo University, 2015 (unpublished).
- [40] C. Young, *Phys. Rev. C* **89**, 024913 (2014).
- [41] K. Murase and T. Hirano, [arXiv:1304.3243](https://arxiv.org/abs/1304.3243).
- [42] K. Murase and T. Hirano, *Nucl. Phys. A* **956**, 276 (2016).
- [43] M. Singh, Characterizing the quark gluon plasma using soft thermal fluctuations and hard parton interactions, Ph.D. thesis, McGill University, 2021 (unpublished).
- [44] A. Sakai, K. Murase, and T. Hirano, *Phys. Rev. C* **102**, 064903 (2020).
- [45] A. Sakai, K. Murase, and T. Hirano, *Phys. Lett. B* **829**, 137053 (2022).
- [46] K. Kuroki, A. Sakai, K. Murase, and T. Hirano, *Phys. Lett. B* **842**, 137958 (2023).
- [47] K. Murase, *Ann. Phys. (NY)* **411**, 167969 (2019).
- [48] T. Hirano, R. Kurita, and K. Murase, *Nucl. Phys. A* **984**, 44 (2019).
- [49] P. E. Kloeden and E. Platen, *Numerical Solution of Stochastic Differential Equations* (Springer, Heidelberg, 1992).
- [50] A. Bazavov *et al.* (HotQCD Collaboration), *Phys. Rev. D* **90**, 094503 (2014).
- [51] P. K. Kovtun, D. T. Son, and A. O. Starinets, *Phys. Rev. Lett.* **94**, 111601 (2005).
- [52] F. Cooper and G. Frye, *Phys. Rev. D* **10**, 186 (1974).
- [53] D. Teaney, *Phys. Rev. C* **68**, 034913 (2003).
- [54] A. Monnai and T. Hirano, *Phys. Rev. C* **80**, 054906 (2009).
- [55] B. Ling, T. Springer, and M. Stephanov, *Phys. Rev. C* **89**, 064901 (2014).
- [56] J. I. Kapusta and C. Plumberg, *Phys. Rev. C* **97**, 014906 (2018); **102**, 019901(E) (2020).
- [57] A. De, C. Plumberg, and J. I. Kapusta, *Phys. Rev. C* **102**, 024905 (2020).
- [58] H. Fujii and M. Ohtani, *Phys. Rev. D* **70**, 014016 (2004).
- [59] D. T. Son and M. A. Stephanov, *Phys. Rev. D* **70**, 056001 (2004).
- [60] A. Sakai, K. Murase, H. Fujii, and T. Hirano, *Acta Phys. Pol. Suppl.* **16**, 1 (2023).